Aalto University
School of Chemical
Technology

School of Chemical Engineering

Degree Programme of Bioproducts and Biosystems

Most Kaniz Moriam

CORRECTED GIBBS-THOMSON COEFFICIENT FOR THE CELLULOSE-CYCLOHEXANE SYSTEM

Master's thesis for the degree of Master of Science in Technology
submitted for inspection, Espoo, 11.08.2017

Supervisor **Professor Thaddeus Maloney**

Instructor **M.Sc. Sara Ceccherini**

Aalto University
School of Chemical
Engineering

Aalto University, P.O. BOX 11000, 00076
AALTO
www.aalto.fi

Abstract of master's thesis

Author:	**Most Kaniz Moriam**
Title of thesis:	**Corrected Gibbs-Thomson coefficient for the cellulose-cyclohexane system**
Degree Programme:	**Master's Programme in Chemical, Biochemical and Materials Engineering**
Major:	**Fibre and Polymer Engineering**
Thesis supervisor:	**Professor Thaddeus Maloney**
Thesis advisor(s) / Thesis examiner(s):	**Sara Ceccherini**
Date 11.08.2017	**Number of pages** 75+23 **Language:** English

Abstract

Thermoporosimetry is a calorimetric method that allows the measurement of the pore size distribution (PSD). The method measures the melting or freezing point depression of a liquid trapped in a pore. Then, this melting/freezing point depression is correlated to the pore size by the Gibbs-Thomson coefficient. Thermoporosimetry has several advantages. For example, it does not require toxic chemicals. Compared to other methods, the sample preparation is relatively simple. Moreover, samples analysis occurs in wet-state.

However, the application of thermoporosimetry to cellulosic materials presents some critical limitations. Instead of using pulp fibers, the Gibbs-Thomson coefficients are calculated from materials with a different porosity, such as, silica or controlled porous glass material. This might provide misleading pore information. Thus, the primary aim of this work was to overcome this limitation. By combining cyclohexane thermoporosimetry and Hg-porosimetry, a system for determining an alternative Gibbs-Thomson coefficient was presented for a set of five types of pulps. These included bleached/unbleached, hardwood/softwood, and dried/never dried fibers. Additionally, by combining thermoporosimetry and centrifugation method, a novel platform was developed to estimate the amount of true macropores in fiber cell wall.

In conclusion, a framework for calculating 'corrected' Gibbs-Thomson coefficient for thermoporosimetry-based PSD determination in cellulose-cyclohexane system was demonstrated in this study. Furthermore, thermoporosimetry was applied to quantify fiber cell wall macropores.

Keywords: Thermoporosimetry, Gibbs-Thomson coefficient, pore size distribution, cellulose, Macropore

PREFACE

The Master's thesis project was carried out in the Department of Bioproducts and Biosystems, Aalto University from January-May, 2017.

This study was completed under the supervision of Professor Thaddeus Maloney. I would like to thank Professor Thaddeus Maloney for offering me the opportunity, facilities and funding for the master's thesis. His encouragements, educational supervision and extended patience throughout the project helped me complete the thesis work.

I owe my warmest thanks especially to Sara Ceccherini for her advices and suggestions during the thesis writing.

In addition, I am very grateful to Josphat Phiri, Jonna Kuusisto, Leena Nolvi, Tuyen Nguyen for their kind support during the entire study. I am thankful to Kaarlo Nieminen for helping me in the mathematical calculations.

I owe my great thanks to my study tutor Eero Hiltunen for his encouragement and advice.

Finally, I would like to thank Finnish Cultural Foundation for partially covering the expenses for this Master's thesis project.

Espoo, 11th August, 2017

Most Kaniz Moriam

Table of Contents

1. Introduction

Cellulose fibers contain porous structures intrinsically (Park, Venditti et al. 2006). Pores can be also introduced by various chemical and mechanical treatments. For example, processes such as pulping and bleaching enrich fiber porosity removing hemicellulose and lignin (Park, Venditti et al. 2006).

The porous structure of cellulose fibers governs many important properties, such as accessibility and reactivity (Miao, Chen et al. 2014), rheology and swelling (Dimic-Misic, Puisto et al. 2013), enzymatic hydrolysis (Grönqvist, Hakala et al. 2014), and chemical modifications (Aarne, Kontturi et al. 2012). Thus, an accurate determination of fiber pore structure is essential.

Thermoporosimetry is a well-known pore analysis method, where pore structure can be measured in wet-state (Hay, Laity 2000, Riikonen, Salonen et al. 2011a). This method considers the depressed melting point of absorbate held in a porous material. The melting temperature depression correlates with the pore size using Gibbs-Thomson coefficient (Maloney, Paulapuro 1999, Wulff 2004a).

Until now, Gibbs-Thomson coefficient for cellulosic fibers has been calculated using silica and controlled porous glass as reference (Maloney 2015, Książczak, Radomski et al. 2003a, Maloney 1999). However, the pore structure of cellulosic fibers differs from that of these reference materials. In fact, the pore structure of silica and porous glass is rigid and defined, whereas that of cellulose fibers contains overlapping pore structure. Furthermore, the pore structure of hard materials is intact both at the frozen and liquid states. On the other hand, cellulose is a soft material, and it can expand or shrink during freezing. Hence, the use of silica and glass porous materials for the calculation of the

Gibbs-Thomson coefficient can provide some misleading information about the pore size distribution of the cellulosic fibers (Maloney 2015).

Considering these limitations, the present thesis work aimed to provide reasonable correction of the Gibbs-Thomson co-efficient for the cellulosic fibers. Cellulosic fibers were used as a reference material for calculating Gibbs-Thomson coefficient. The porosity of the cellulosic fibers and porosity characterizing techniques, such as thermoporosimetry, N_2 sorption, Hg-porosimetry, solute exclusion method, water retention value, and cyclohexane retention value, were discussed in the literature review.

The study investigated hardwood and softwood pulps. The experimental part was sub-divided into 3 distinct steps: i) characterization of the pulps and porosity measurements, ii) comparison of the porosity measurements from various methods and macropore quantification and iii) an alternative Gibbs-Thomson coefficient calculation based on thermoporosimetry and Hg-porosimetry.

Although further investigation is necessary, this study demonstrated a promising procedure for overcoming the existing limitations that affect the thermoporosity-based pore size distributions of cellulosic pulps.

2. LITERATURE REVIEW

2.1. Wood fibers

Softwood and hardwood are two subdivisions of wood. Softwoods contain 90-95% of longitudinal tracheid and a small amount of ray cells. On the other hand, hardwoods consist of libriform fibers, vessels and ray cells (Rowell, Pettersen et al. 2005, Sjöström 1993).

Softwood tracheids are long (length 2-4 mm) and narrow (width 0.02-0.04 mm). Libriform fibers of hardwood are shorter (1.1-1.2 mm) than softwood tracheids, and their average width is 0.014-0.04 mm. The vessels elements are shorter (0.3-0.6 mm) than hardwood fibers having width of 0.03-0.13 mm (Sjöström 1993).

2.1.1. Composition of fiber cell wall

The fiber cell wall is primarily constituted by cellulose, hemicellulose and lignin. Cellulose gives strength to the cell wall, hemicellulose controls the amount of water in the cell wall, and lignin acts as a glue between the cell walls (Pönni, Vuorinen et al. 2012a).

Cellulose and hemicellulose are polysaccharides. Molecular weight of hemicellulose is lower than cellulose. Lignin is a complex polymer cross-linked with phenyl propane (Sjostrom 2013). The quantity and composition of lignin and hemicelluloses are different in softwood and hardwood. By contrast, the amount of cellulose is equal in both woods (Koch 2008).

2.1.2. Cell wall structure

Fiber cell wall structure contains three main layers respectively named middle lamella, primary wall and secondary wall (Figure 1) (Berry, Roderick 2005, Sjostrom 2013, Rowell, Pettersen et al. 2005).

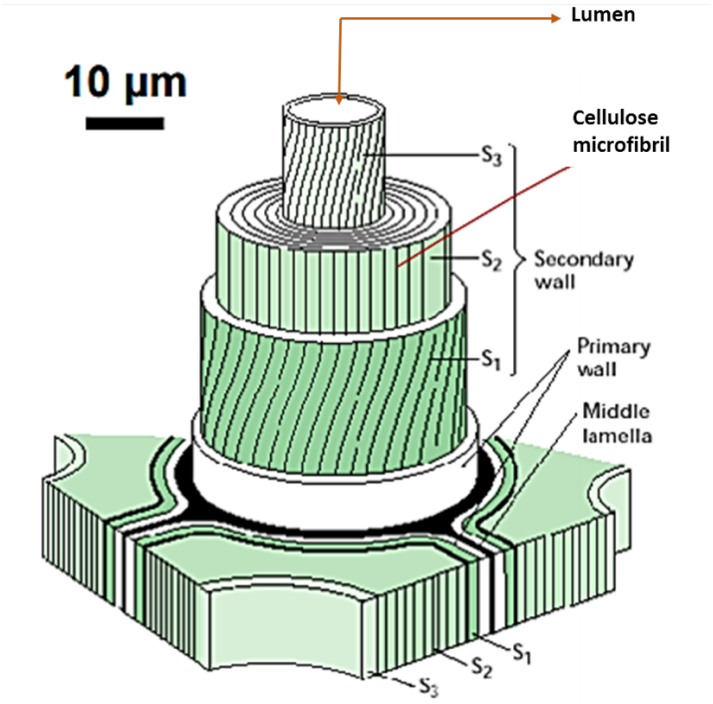

Figure 1. Schematic model of layers in cell wall (Plomion, Leprovost et al. 2001)

The outermost layer is called middle lamella, and its thickness measures 0.1-0.2 µm. The middle lamella is mainly composed of pectin, which shows high affinity to water. Sometimes, the middle lamella cannot be distinguished from the adjacent primary wall. Then, the term "compound middle lamella" is used to describe both of them (Fengel, Wegener 1983).

The primary cell wall consists of lignin, pectin, hemicellulose, and a small amount of irregularly oriented cellulose microfibrils (Rowell, Pettersen et al. 2005). Moreover, the

amount of lignin is higher in this layer rather than in the other layers of cell wall (Fahlén 2005).

The secondary wall involves three distinct layers, S_1, S_2 and S_3 (Figure 1). These layers extend from the primary cell wall until the inner cavity of the fiber, which is named lumen.

S_1, S_2, and S_3 show different thicknesses and fibril angles, which are the angles between the microfibrils and the fiber axis (Rowell, Pettersen et al. 2005). The S_2 layer is the thickest layer having thickness of 1-5 μm compared to the S_1 (0.2-0.3 μm) and S_3 (~ 0.1 μm) (Sjöström 1993). The fibril angle of S_2 layer (0-30°) is lower than that of both S1 (50°-70°) and S3 layer (50°-90°). The low fibril angles of S2 prevent fiber swelling or shrinkage along the longitudinal direction (Rowell, Pettersen et al. 2005, Sjostrom 2013, Sjöström 1993).

2.2. Cellulose

Cellulose is the major component of plant cell wall. It has syndiotactic linear polymer structure which consists of 1-4-linked β-D anhydroglucopyranose unit (Figure 2).

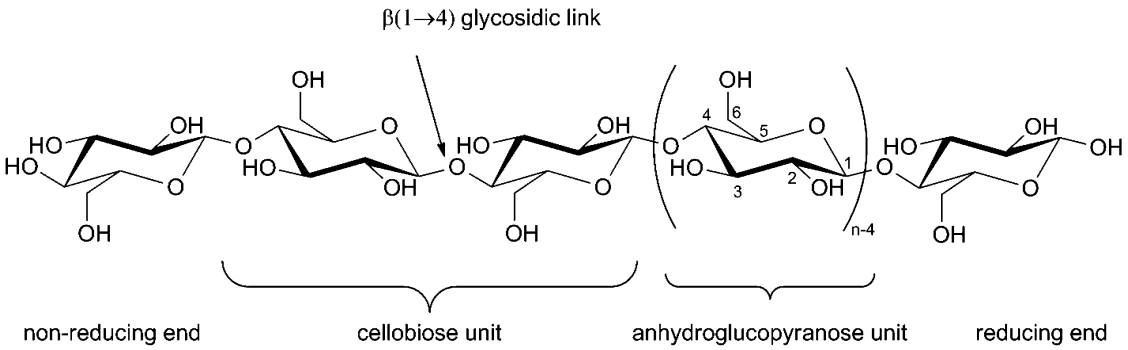

Figure 2: The linear polymeric structure of cellulose is arranged into 1-4-linked β-D anhydroglucopyranose unit (Eyley, Thielemans 2014).

The C-1 end of this polysaccharide is considered as reducing end, because the anomeric carbon is not involved in glycosidic bondage. However, the hydroxyl group in C-4 end is non-reducing (Varshney, Naithani 2011). Each monomeric unit possesses three hydroxyl groups in C2, C3 and C6 position. These hydroxyl groups are involved in hydrogen bond network (Hallac, Ragauskas 2011a).

The number of monomeric units and the degree of polymerization (DP) of cellulose depends on its origin. In general, the DP of plant fibers cellulose lies within a range of 800-10000 (Klemm, Heublein et al. 2005). However, the DP of cellulose derived from hardwood, softwood and dissolving pulps are 3500-4500, 1450-1500 and 650-1000, respectively (Sweet, Winandy 1999, Hallac, Ragauskas 2011b). The DP determines the different properties of cellulose. Lower DPs reduce the viscosity and enhance the process ability, whereas high DPs improve the mechanical properties of the cellulose derivatives (Varshney, Naithani 2011).

The presence of β- linkage causes flipped or ribbon-like structure in cellulose. This kind of structure contributes inter- and intra-molecular hydrogen bonds. The ribbon-like structure builds up into sheet, which are held in staggered layers by weak van der Waals forces (Nevell, Zeronian 1985).

Cellulose contains both amorphous and crystalline regions (Figure 3). Water is inaccessible to the crystalline part, but accessible to the amorphous part (Khalil, Davoudpour et al. 2016).

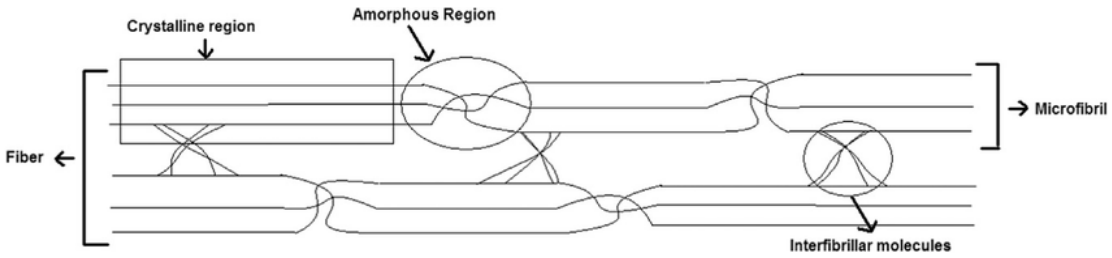

Figure 3: Schematic representation of the crystalline and amorphous regions of cellulose (Khalil, Davoudpour et al. 2016)

Cellulose exists in different crystalline forms, which are known as polymorphs. These polymorphs include cellulose I, II, III-1, III-2, IV-1 and IV-2. However, cellulose I and II can be considered the most relevant as they can convert into all the other polymorphs using different treatments (Malcolm Jr, Saxena 2007).

Cellulose I is native cellulose containing crystalline regions characterized by parallel chain orientation. This polymorph includes two subgroups called I_α and I_β. Cellulose I_α is distinguished by a single chain triclinic unit cell, and it is dominant in bacteria and algae. On the other hand, cellulose I_β has a two-chains monoclinic unit cell, and it is present in higher plants.

Cellulose II, called also “regenerated cellulose”, is characterized by an antiparallel chain orientation. Celluose II can be derived by mercerization or regeneration of native cellulose (Ciolacu, Pitol-Filho et al. 2012, Rowell, Pettersen et al. 2005)

2.3. Porous Structure of fibers

The fiber cell wall is composed of cellulose microfibrils, which are surrounded by the matrix of hemicellulose and lignin. The length of microfibrils extend to several micrometers, while the width ranges between 2 and 20 nm.

The intra-lamellar spaces between the microfibrils and the lignin-hemicellulose matrix originate pores in the fiber cell wall. In nature, due to the presence of water, pores remain in swollen state (Aarne 2013). Pulping process involves the removal of lignin and hemicellulose, which leads to an increasing porosity (Figure 4) (Fahlén 2005, Stone, Scallan 1965, Lindström 1986, Andreasson, Forsström et al. 2003).

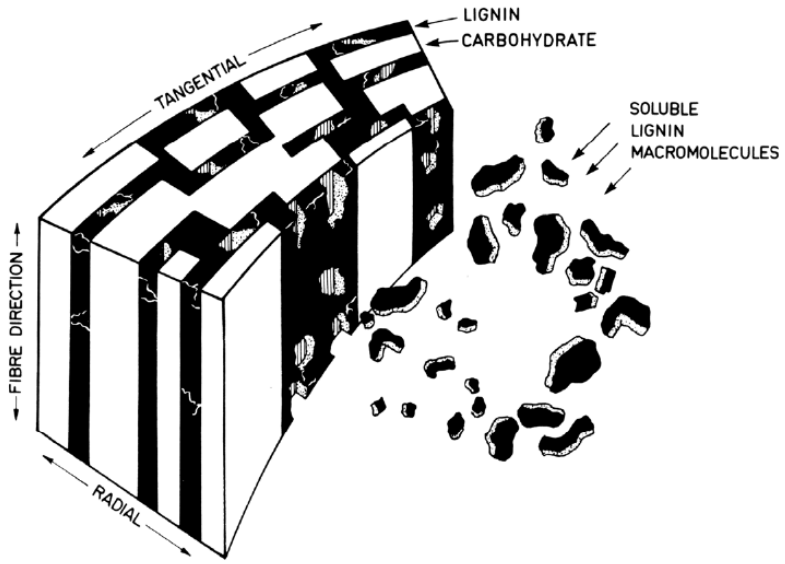

Figure 4: Schematic of delignification and formation of cell wall pores (Goring 1977)

The pores are arranged along the transverse direction of fiber cell wall. Multiple factors, such as chemical composition, degree of crystallinity and fiber charge groups, can modulate pore size (Aarne 2013).

2.4. Measurement of porous materials

Pore analysis provide information about the geometry of the pores including size, shape and arrangement; pore volume, pore size distribution and other related information (Maloney, Paulapuro 1999). Pore measurements can be performed using several methods, such as N_2 sorption (Kimura, Qi et al. 2016), Hg extrusion (Gane, Ridgway et al. 2004), solute exclusion (Lovikka, Khanjani et al. 2016), nuclear resonance spectroscopy (NMR) (Mitchell, Webber et al. 2008a), and thermoporosimetry (Maloney 2015).

2.4.1. Thermoporosimetry

Recently, thermoporosimetry (TPM) has received considerable attention as an efficient method for analyzing porous materials. This method measures the pore size distribution (PSD) considering the depressed melting point corresponding to the liquid confined in the pores rather than in the bulk liquid (Figure 5) (Maloney 2015, Landry 2005, Ishikiriyama, Todoki 1995).

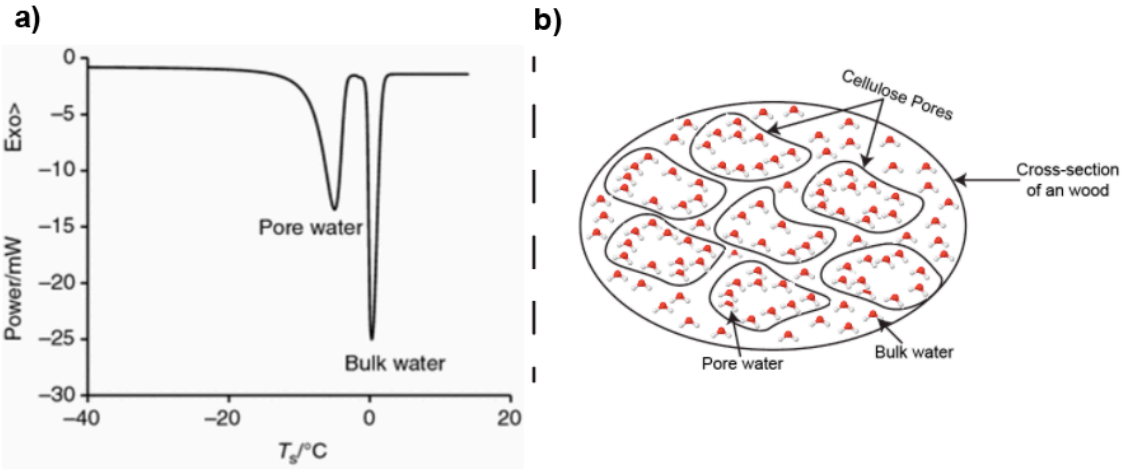

Figure 5: a) Melting of pore and bulk water in silica (Maloney 2015), and b) schematic diagram of distribution of pore water and bulk water in a cross section of wood.

This depression of melting point is the result of lower pressure at the curved interface of the pore. Gibbs-Thomson coefficient is the correlation coefficient that allows to calculate pore size distributions from melting temperature depression data in Differential Scanning Calorimetry (DSC) analysis.

TPM is especially useful to analyze cellulosic material as it represents a wide range of information about fiber pores from saturated state to wet state (Maloney 2015). Measuring porosity in wet state provides TPM a unique advantage over other pore measuring methods, because pores are prone to collapse and aggregate upon drying (Park, Venditti et al. 2006).

2.4.1.1. Gibbs-Thomson coefficient

The Gibbs-Thomson equation represents the inverse relationship between the shift of the melting point and the pore size distribution. The equation can be expressed as:

$$D = \frac{K}{\Delta T} + t \qquad (1)$$

Where, K is the Gibbs-Thomson coefficient in nm°C and t is the thickness (nm) of the non-freezing liquid layer (Maloney 2015).

Gibbs-Thomson coefficient has been calculated for several materials, such as porous silica and similar well-behaved materials, including cellulose (Table 1) (Ishikiriyama, Todoki et al. 1995, Majda, Makowski et al. 2015, Wulff 2004a). However, in case of complex pulp fibers and other cellulosic materials, Gibbs-Thomson-based PSD calculations are generally inaccurate and require further investigation (Maloney 2015).

Table 1 : Gibbs-Thomson coefficient and non-freezing coefficient values from literature

Analyzed samples	**Gibbs-Thomson coefficient (nm°C)**	**Non-freezing coefficient (nm)**
SBA-15 in water (Yamamoto, Endo et al. 2005)	64.70 (freezing)	0.23 (freezing)
HCP (hardened cement paste)(Pastorino, Canal et al. 2015)	64.67 (freezing) 32.33 (melting)	0.57(freezing) 0.68 (melting)
nitrocellulose in water (Książczak, Radomski et al. 2003b)	64.67 (Freezing) 32.33 (melting)	0.57 (Freezing) 0.68 (melting)
nitrocellulose in Benzene (Książczak, Radomski et al. 2003b)	131.60 (Freezing) 65.80 (melting)	1.76 (Freezing) 2.94 (melting)
CPG in water(Landry 2005)	19.08 (melting) 38.56 (freezing)	0.12(melting) 0.17 (freezing)
silica gel in water(Landry 2005)	33.30 (melting) 56.36 (freezing)	0.32 (melting) 0.90 (freezing)
Polystyrene/ Divinylbenzene(DVB) (Wulff 2004b)	309.00 (melting)	13.00 (melting)
Bacterial Cellulose (Kaewnopparat, Sansernluk et al. 2008)	38.56 (melting)	0.30 (melting)
Poly methyl methacrylate (PMMA) hydrogel in water (Ishikiriyama, Todoki et al. 1995)	56.36 (freezing) 33.30 (melting)	0.90 (freezing) 0.32 melting)

2.4.1.2. Gibbs-Thomson coefficient derivation

Every porosimetry is based on the theory of inter-connection between the solid, liquid and gas phase (Defay, Prigogine et al. 1966, Brun, Lallemand et al. 1977). When phase transitions occur in capillary systems, the surface tension plays a crucial role to maintain the equilibrium among mechanical, thermal and chemical energy changes. According to the Laplace theory, the pressure difference between two phases is balanced by interfacial tension between the two phases that is acting tangentially. This can be described by the following equation:

$$P_j - P_i = \gamma_{ij} \frac{dA_{ij}}{dV_j} \quad (2)$$

Here, P_j and P_i are the pressure of two arbitrary phase i and j, while dA_{ij}/dV_j is the arbitrary curvature between two arbitrary phase i and j.

According to Gibbs-Duhem equation, the equilibrium state between different bulk phases can be expressed as follows:

$$S_s\delta T - V_s\delta P_s + n_s\delta\mu_s = 0 \quad (3)$$

$$S_l\delta T - V_l\delta P_l + n_l\delta\mu_l = 0 \quad (4)$$

$$S_g\delta T - V_g\delta P_g + n_g\delta\mu_g = 0 \quad (5)$$

Where, the subscripts s, l and g express solid, liquid and gas, respectively. δT is temperature change, δP is change in pressure and δμ is change in chemical potential. S, V and n refer to entropy, volume and number of moles (Defay 1966).

Laplace equation (2) can express the thermodynamic balance in following ways:

$$P_l - P_g = \gamma_{lg}\left(dA_{lg}/\, dV_l\right) \tag{6}$$

$$P_g - P_s = \gamma_{gs}\left(dA_{gs}/\, dV_g\right) \tag{7}$$

$$P_s - P_l = \gamma_{sl}\left(dA_{sl}/dV_s\right) \tag{8}$$

Gibbs phase rule suggests the presence of two independent degrees of freedom for curved interface among three bulk phases (Defay, Prigogine et al. 1966). In thermoporosimetric experiments, excess liquid is added to ensure complete filling of pores. The excess solid (ice) creates a planner surface at any temperature lower than the equilibrium temperature (Figure 6).

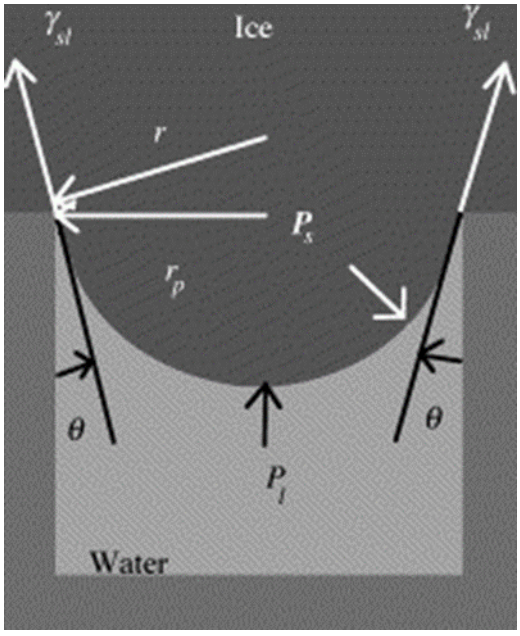

Figure 6: The consideration for thermoporosimetry when excess liquid is added to the porous sample. $\boldsymbol{\theta}$ is the contact angle, γ_{sl} is the surface tension of solid-liquid and r_p is the pore radius (Landry 2005).

In this situation, solid-liquid and gas-solid interface can be considered. The differentiation of equation (7) and (8) can express as:

$$\delta P_g - \delta P_s = \delta(\gamma_{gs} * dA_{gs}/ dV_g) \quad (9)$$

$$\delta P_s - \delta P_l = \delta (\gamma_{sl} * dA_{sl}/ dV_s) \quad (10)$$

For solid-liquid interface, equation (3) is subtracted from equation (4):

$$\left(\frac{S_s - S_l}{V_s - V_l}\right) \delta T = \frac{V_s}{V_s - V_l} \delta P_s - \frac{V_l}{V_s - V_l} \delta P_l \quad (11)$$

And equation (3) is subtracted from equation (5) considering gas-solid surface:

$$\left(\frac{S_g - S_s}{V_g - V_s}\right) \delta T = \frac{V_g}{V_g - V_s} \delta P_g - \frac{V_s}{V_g - V_s} \delta P_s \quad (12)$$

Again, following equation is obtained by subtracting equation (11) from (12) and substituting of values of δP_g (from equation 9) and δP_l (from equation 10)-

$$\left[\left(\frac{S_s - S_g}{V_s - V_g}\right) - \left(\frac{S_l - S_s}{V_l - V_s}\right)\right] \delta T = \frac{-V_g}{V_s - V_g} \delta \left(\gamma_{gs} \frac{dA_{gs}}{dV_g}\right) + \frac{V_l}{V_l - V_s} \delta \left(\gamma_{sl} \frac{dA_{sl}}{dV_s}\right) \quad (13)$$

Here, $dA_{gs}/dVg = 0$, for the planar gas –solid surface.

When $v_g >> v_l, v_s$, then $v_g >> (v_l - v_s)$. Hence, equation (13) becomes:

$$(s_l - s_s)\delta T = -2v_l\gamma_{sl}\delta(1/r_{sl}) \quad (14)$$

At a certain temperature interval, the correlation between entropy change and molar heat of fusion can be expressed as-

$$(s_l - s_s)T = \Delta h_f \quad (15)$$

Combining equation (14) and equation (15) followed by further integration from T_0 to T, the thermoporosimetry relationship can be obtained-

$$ln\frac{T}{T_0} = -\frac{2V_l\gamma_{sl}}{\Delta h_f r_{sl}} \quad (16)$$

ln (T/T_0) can be expanded as-

$$ln\ (T/T_0) = ln\ (T_0\text{-}\Delta T)/T_0 = ln\ (1\text{-}\ \Delta T/\ T_0) \approx -\Delta T/T_0 \quad (17)$$

Specific molar volume, $v_l = M/\rho_l$ where, M is the molecular weight of liquid and ρ_l is the density of liquid and molar heat of fusion $\Delta h_f = \Delta H_f/M$, where ΔH_f apparent heat fusion; $r_{sl} = r_p/cos\boldsymbol{\theta}$ according to Laplace equation. Finally, insertion of the values for v_l, Δh_f, r_{sl} and ln (T/T_0) gives the final equation-

$$\Delta T = \frac{2\ To^{\gamma}sl\ cos\theta}{\rho l\ \Delta Hf\ rp} \quad (18)$$

Pore radius, $r_p = D/2$, inserting this value equation (18) can be written as-

$$\Delta T = \frac{4\ To^{\gamma}sl\ cos\theta}{\rho l\ \Delta Hf\ D} \quad (19)$$

Existence of non-freezing liquid layer gives relationship between temperature difference and pore radius-

$$\Delta T = \frac{4To^{\gamma}sl\ cos\theta}{\rho l\ \Delta Hf\ (D-t)} \quad (20)$$

Equation (21) is analogous to the Gibbs-Thomson equation (1). Here, t is the thickness of non-freezing liquid layer. However, the heat of fusion, the density, the surface tension and the contact angles are practically very difficult to measure independently.

2.4.1.3. Non-Freezing liquid layer

Non-freezing water is the fraction of water in the pores which does not undergo water-ice or ice-water phase transition when the temperature reaches the melting or freezing point of the bulk water (Riikonen, Salonen et al. 2011b, Landry 2005, Endo, Yamamoto et al. 2008a). Different studies explain the reason behind the non-freezing behavior of water (Galin, Galin 1992, Maloney, Paulapuro et al. 1998, Stapf, Kimmich et al. 1996).

Berlin et al (1970) suggested that the first 1-3 layers of water adjacent to the surface does not freeze due to the resemblance of ice configuration. Additional reason might be the limited motion of those water molecules (Berlin, Kliman et al. 1970). Ishikiriyama and Todoki (1995a) calculated the thickness of 0.4-0.8 nm for non-freezing water consisting of two or three monolayers. The most common range for the layer was reported to be 0.5 to 0.8 nm (~2-3 monolayers) (Endo, Yamamoto et al. 2008b, Riikonen, Salonen et al. 2011b). The water molecules in the first layer of the surface are oriented by electrostatic or hydrogen bonding interactions (Maloney, Paulapuro et al. 1998). By contrast, some studies showed that the motion of the water molecules in outmost non-freezing layer was indistinguishable from the motions in bulk water (Galin, Galin 1992, Stapf, Kimmich et al. 1996).

According to Deodhar and Luner (1980), the water does not freeze within a minimum pore size (4 nm at -4°C) (Deodhar, Luner 1980). Crystallization is the formation of crystals, and it is a phenomenon during freezing (Kiani, Sun 2011). The crystallization might be prevented into small pores within a certain range, because sufficient liquid molecules cannot access into small pores to generate nucleation for crystallization. This phenomena is called ‘stacking faults’(Wu, Zheng et al. 2014). The stacking faults reduce with larger pore sizes, and it can be negligible over 100 nm (Riikonen, Salonen et al. 2011b).

In addition, another study suggested that, the non-freezing behavior of water is related to the kinetic effects. This kinetic effect describes the slow diffusion of water which resist the ice formation either at the low temperature (-12°C for pulps) or low moisture content (about 0.25 g/g) (Maloney, Paulapuro et al. 1998). Furthermore, some studies indicated that, the non-freezing water is interconnected with the number of accessible hydroxyl group (Nakamura, Hatakeyama et al. 1981a).

2.4.1.4. Use of Differential Scanning Calorimetry for thermoporosimetry

Differential Scanning calorimetry can use two kinds of melting methods: dynamic melting method and isothermal step melting method (Figure 7).

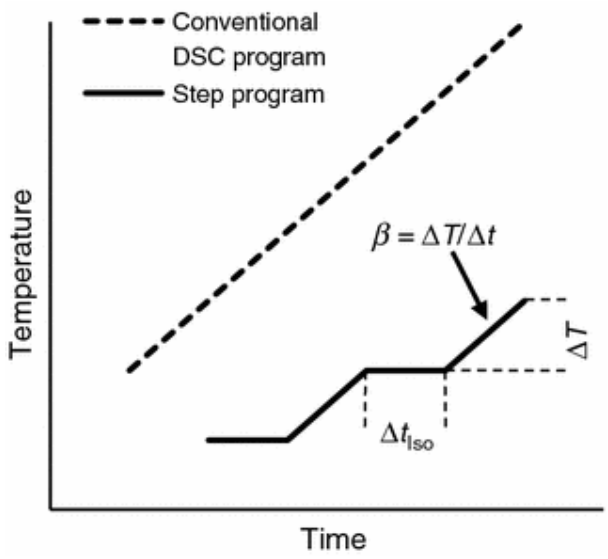

Figure 7: Schematic of conventional dynamic melting method and isothermal step melting method. β is the heating rate and Δt_{iso} is the isothermal segment (Maloney 2015).

While the dynamic melting method heats the sample at a constant heating rate, the step melting method rises the temperature stepwise. At each step, the temperature remains constant until thermal equilibrium is attained. This constant temperature step is known as "isothermal segment".

On the other hand, step melting method is used for macropore containing soft porous materials, such as cellulose fibers. This step melting method can overcome thermal lag problem, which arises from the temperature difference between the sample and the measurement sensors. Due to this thermal lag, melting point depression peaks overlap with the melting peak of bulk liquid (Figure 8).

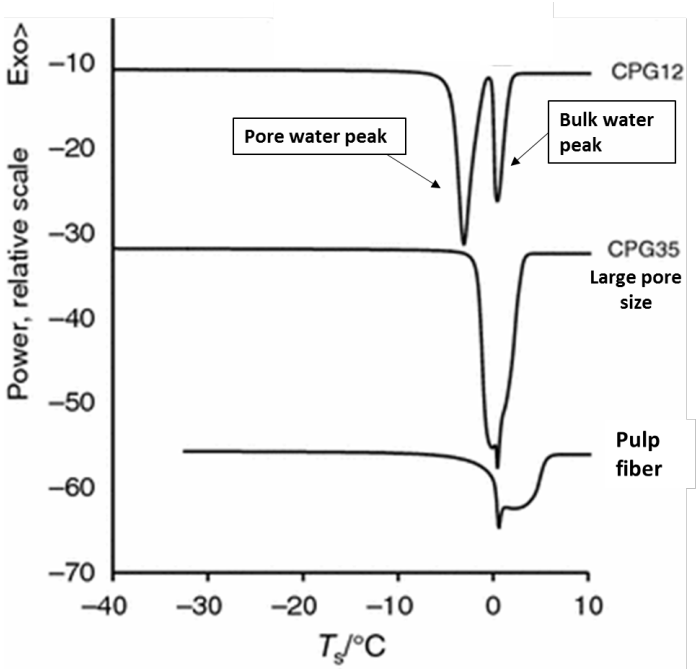

Figure 8 : Comparison of the endothermic DSC curves relative to porous glass with small pores, porous glass with large pores, and pulp fiber (Maloney, Paulapuro 2001).

Hence, pore volume calculations become challenging, because each peak cannot be integrated separately. In step melting method, an isothermal condition is maintained, and the peaks are visualized separately (Maloney 2015, Maloney 1999).

2.4.1.5. Pore size distribution (PSD) measurement

Melting point depression converts into pore diameter using the relation from Gibbs Thomson equation (1). The Gibbs Thomson coefficient (K) is solvent specific. According to the literature, the K for water and cyclohexane could measure 42-43 nm°C (Nakamura, Hatakeyama et al. 1981b, Maloney 2015) and 117 nm°C, respectively (Maloney, Paulapuro 2001).

PSD calculations use the isothermal step melting method, and all the peaks are integrated accurately (Figure 9). The area of each step melting peak is the sum of sensible and latent

heats. Latent heat is related to the heat required for phase changes, whereas sensible heat is the temperature changes when no phase change occurs (Farid, Khudhair et al. 2004).

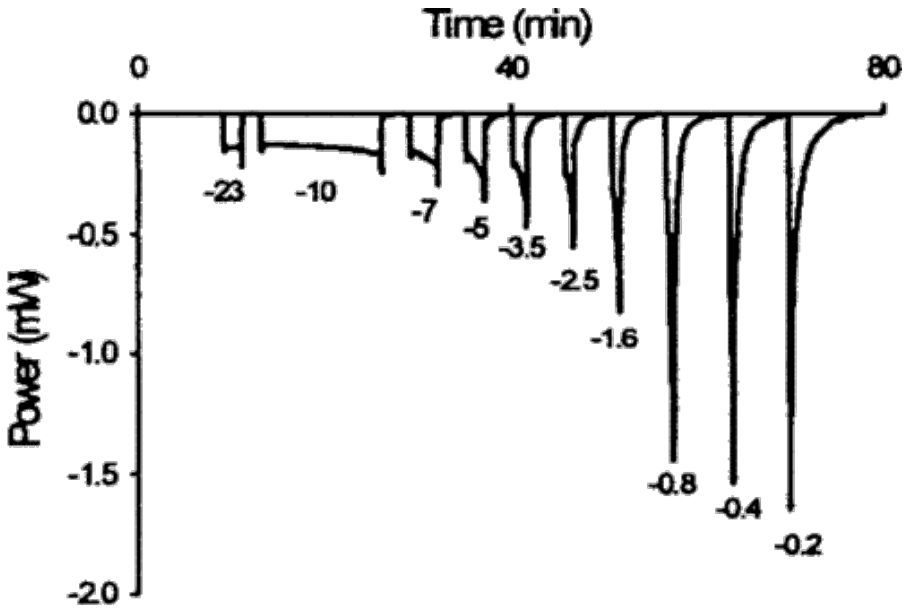

Figure 9 : Example of step melting curve for fibers in water (Maloney, Paulapuro 2001).

The amount of melted liquid is calculated by means of the latent heat. Usually, the first isothermal segment is chosen in such a way where no phase transition happens. The heat of the first step is considered as a sensible heat. This sensible heat is subtracted from heat of each other step to obtain total latent heats. The latent heat is calculated using following equation:

$$H_{LN} = H_{TN} - H_{T1}\frac{\Delta T_n}{\Delta T_1} \quad (21)$$

Where, H_{LN} is the total latent heat, H_{TN} is the total heat of the steps, H_{T1} is the heat of first step, ΔT_1 and ΔT_n are the size of step 1 and the size of step n, respectively.

Then, H_{LN} can be converted into total pore volume (V_n) using following equation:

$$V_n = \frac{H_{LN}}{H_m W} \quad (22)$$

Here, W is the dry matter content of the sample, while H_m is the melting heat for bulk material in J/g. H_m for water and cyclohexane are respectively estimated 334.5 J/g and 30.07 J/g (Maloney, Paulapuro 2001). Non-freezing liquid is calculated by the subtraction of the amount of freezing liquid from the total content of liquid in the sample (Wang 2006).

2.4.1.6. Comparison of Cyclohexane and water as absorbate in thermoporosimetry

In TPM, absorbate cyclohexane offers several advantages over water. While water is a polar solvent, cyclohexane is a non-polar organic solvent. Consequently, it does not swell fibers, because its interaction with fibers are weak. Moreover, cyclohexane prevents fibers from being damaged by freezing. At frozen state, water forms hard ice crystals, whereas cyclohexane soft crystals. In addition, due to thermodynamic difference, cyclohexane-based TPM method can measure pore sizes up to 600 nm, while water-based TPM pore sizes reach a maximum of ca. 200 nm (Maloney, Paulapuro 2001, Wang 2006). In water-based TPM, the melting point depression might occur due to the resultant osmotic pressure exerts either by partial dissolution of cell wall polysaccharides or presence of ions. This can introduce inaccuracy during measurement. On the other hand, cyclohexane-based TPM can avoid this misleading information (Wang 2006).

However, cyclohexane TPM reported some shortcomings. For example, the contraction of microfibrillated cell wall is occurred due to the removal of osmotic pressure (Wang 2006). Additionally, cyclohexane-based TPM is ten times more sensitive than water-

based TPM. The latent heat of cyclohexane (30.07 J/g) is ten times lower than water (334.5 J/g) (Maloney, Paulapuro 2001).

2.4.2. Nitrogen (N_2) sorption porosimetry

N_2 sorption porosimetry is a method that measures both the surface area and the porosity of solid porous structure. This porosimetric technique is based on the physisorption of anadsorbable gas on the solid surface. Finally, pores are classified in three categories: micropores (pore width <2 nm), mesopores (pore width 2-50 nm) and macropores (pore width >50 nm) (Sing 2009).

The penetration of gas molecules into the surface layer and bulk solid is called adsorption, while the opposite process is called desorption. Adsorption hysteresis is due to the difference in adsorption and desorption isotherms (Matthias, Katsumi et al. 2015).

Before N_2 sorption analysis, samples are dried using suitable methods. Then, they are exposed to liquid N_2 into the measurement device. N_2 sorption isotherms are obtained by measuring the amount of N_2 adsorption and desorption over a relative pressure range at the boiling point of nitrogen (77 K). Finally, the isotherms are analyzed to estimate surface areas, pore volumes, and pore size distributions.

The surface area measurement relies on Brunauer-Emmett-Teller (BET) equation:

$$\frac{p}{n(1-p)} = \frac{1}{n_m C} + \frac{C-1}{n_m C} \qquad (23)$$

Where, n is the specific amount of gas adsorbed at the relative pressure p/p^0; n_m is the specific monolayer capacity; p is the relative pressure; and C is the constant related to the average heat of adsorption of the monolayer.

C-constant can be more precisely described as:

$$C = \frac{Exp(q_1 - q_l)}{RT} \quad (24)$$

Where, q_1 and q_2 are the heat of adsorption of the first layer and the heat of condensation, respectively (Ladavos, Katsoulidis et al. 2012). The heat of condensation is equal for all the layers except the first (Quirk 1955). The value of C depends on the shape of isotherm (Sing 2009, Thommes, Cychosz 2014). Usually, it ranges between 50 and 200.

BET specific surface is calculated using following relations:

$$S_{BET} = \frac{n_m * L * \sigma_m}{M_{N_2}} \quad (25)$$

Where, S_{BET} is the BET specific surface area, L is the Avogadro constant, σ_m is the molecular cross sectional area of the adsorbent, and M_{N2} is the molar mass of nitrogen. The molecular cross section of N_2 gas is estimated 0.162 nm^2 at 77K (Emmett, Brunauer 1937).

On the other hand, BET pore volume is calculated according to Gurvich principle (Haul 1982):

$$V_p = q \frac{\rho_{vapor}}{\rho_{liquid}} \quad (26)$$

Here, V_p is the pore volume, q is the volume at saturation ($ml_{STP}\ g^{-1}$), while ρ_{vapor} and ρ_{liquid} are the densities for the vapor phase and liquid phase, respectively. It is assumed that the adsorbed nitrogen has the same density as the liquid phase at saturation. However, this assumption is controversial for microporous materials (Weitkamp, Sing et al. 2002).

Eventually, the PSD of pulp can be measured by Barrett-Joyner-Halenda (BJH) method using solely the adsorption branch of the isotherm. The desorption branch is avoided. In fact, during desorption, mesoporous pores introduce an undesired hysteresis effect from capillary condensed phase (Groen, Peffer et al. 2003).

BJH method assumes that the pores have cylindrical shape and that the total amount of adsorbed N_2 is the sum of adsorption by two different mechanisms. The first mechanism refers to the physical adsorption into the surface layer of the pores. Differently, the second is the adsorption into inner capillary pores by condensation (Barrett, Joyner et al. 1951, De Lange, Vlugt et al. 2014).

According to the BJH method, the pore volume at saturated pressure can be expressed as:

$$V_s = \sum_{i=1}^{k} \Delta V_{p,i}(r_i \leq r_k) + \sum_{i=k+1}^{n} \Delta S_i t_i \, (r_i > r_k) \qquad (27)$$

Here, V_s is the adsorbed gas volume at saturation pressure, r_i is the pore radii, $\Delta V_{p,i}$ are the incremental pore volume which are filled by condensation, ΔS_i are the incremental surface area of the pore which are not completely filled, t_i is the multilayer thickness of the adsorbate, and r_k is the critical radius. The critical radius can be defined as the radius of the largest pore, which is completely filled at certain pressure. Furthermore, BJH method allows to measure the average pore diameter (D_{avg}) for cylindrical pores, where $D_P = 4V_{liquid}$/surface area. However, pulp samples have heterogeneous structure containing both cylindrical and slit-like pores. Slit-like pores give the average diameter, $D_{avg} = 2V_{liquid}$ / surface area. Hence, this consideration can give erroneous values for pulp samples (Kimura, Qi et al. 2014, Kimura, Qi et al. 2016).

2.4.2.1. Classification of physisorption isotherms

Physisorption isotherms are classified into six types: type I, II, III, IV, V & VI (Figure 10). Different types of isotherms are closely related to the specific pore structures (Matthias, Katsumi et al. 2015).

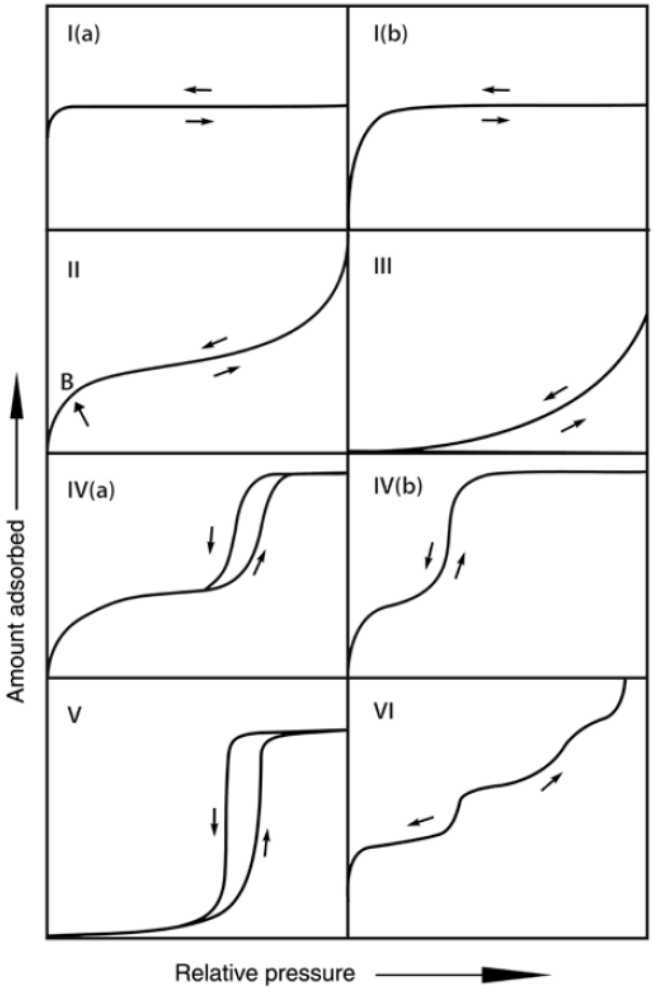

Figure 10 : Different types of physisorption isotherms (Matthias, Katsumi et al. 2015)

Type I isotherm is representative microporous solids. Matthias et al. (2015) presented two subgroups of type I isotherms: I(a) and I(b). While type I(a) results from microporous material having pore width of less than 1 nm, type I(b) is characteristic for the extended micropore widths of <2.5 nm.

Type II isotherm is typical for nonporous or macroporous adsorbents, which are characterized by unrestricted monolayer-multilayer adsorption. The point B indicates the point where multilayer adsorption starts subsequent to the completion of monolayer formation (Figure 10) (Sing 2009).

Type III isotherm is generated by the weak interactions between adsorbent and adsorbate. The adsorbed molecules are arranged on the surface of a nanoporous or macroporous solid. In this isotherm, the B point is indistinctive, because of the overlap of the monolayer with the multilayer adsorption (Sing 2009, Matthias, Katsumi et al. 2015).

Adsorption behavior of mesoporous materials is presented by type IV isotherms. In this case, hysteresis is observed due to the capillary condensation (Figure 10 IVa). Capillary condensation occurs in pores that exceed certain critical width at a certain temperature and pressure. For example, adsorption of nitrogen and argon occurs respectively at 77k and 87 k, and the hysteresis begins at pore size of ≥4 nm (Thommes, Cychosz 2014, Landers, Gor et al. 2013). Differently, type IVb isotherm results from mesoporous adsorbent materials characterized by pores with smaller width or conical and cylindrical mesopores (Matthias, Katsumi et al. 2015).

Isotherm V shows a certain similarity with type III isotherm, such as the weak interaction between adsorbent-adsorbate. However, this isotherm is unusual (Matthias, Katsumi et al. 2015, Sing 2009).

Finally, type VI isotherm represents a stepwise adsorption on uniform non-porous surfaces. This type of isotherm is generated whether the absorbents form a layer-by-layer structure, such as in case of graphitized carbon blacks (Sing 2009, Matthias, Katsumi et al. 2015).

2.4.3. Mercury (Hg) Porosimetry

Mercury porosimetry is a non-wetting method, because the contact angle of mercury with the pore wall is greater than 90°. Hence, this method can avoid any capillary effect. During the measurement, the sample evacuation is performed by addition of liquid mercury. When mercury comes in contact with the porous solid, the gas-liquid surface becomes concave towards the liquid. This concave curvature correlates with the pore size and also explains the higher pressure within the liquid. Thus, external pressure is applied during mercury intrusion to overcome the pressure difference across the curved surface. The pressure (P) required to intrude mercury into pore is inversely related to the pore diameter-

$$D = \frac{-4\gamma_{gl}cos\theta}{P} \quad (28)$$

Here, $^{\gamma}_{gl}$ is the mercury liquid-vapor surface tension of 0.485 Nm^{-1}, and $\boldsymbol{\theta}$ is the contact angle between the liquid mercury and solid surface (Gane, Ridgway et al. 2004, Landry 2005).

2.4.4. Water retention value (WRV)

The WRV method measures the swelling property of pulp fiber (Fahlén 2005). The method assumes that, at certain conditions, centrifugation can effectively remove the water between the fibers. Consequently, the water retained by the fibers after centrifugation corresponds to the swelling of the fiber.

This method is widely appreciated due to its simplicity, reproducibility, accuracy and rapidity. However, WRV results depend on the experimental conditions (Lindström 1986). In addition, further inaccuracy might be caused by the properties of different pulp. This inaccuracy includes the retention of water between the fibers and the removal of cell wall water through pressing (Maloney, Laine et al. 1999).

2.4.5. Solute exclusion method

The solute exclusion method measures the pore volume considering the fiber saturation point (FSP), which is the amount of water that saturates the fiber cell wall and is inaccessible to eventual external probe molecule (Stone, Scallan 1968, Fahlén 2005, Allan, Balaban et al. 1991). If the probe molecules are smaller than the pore, they are accessible to the pore water. However, they cannot penetrate into the pore if they have larger diameter (Figure 11).

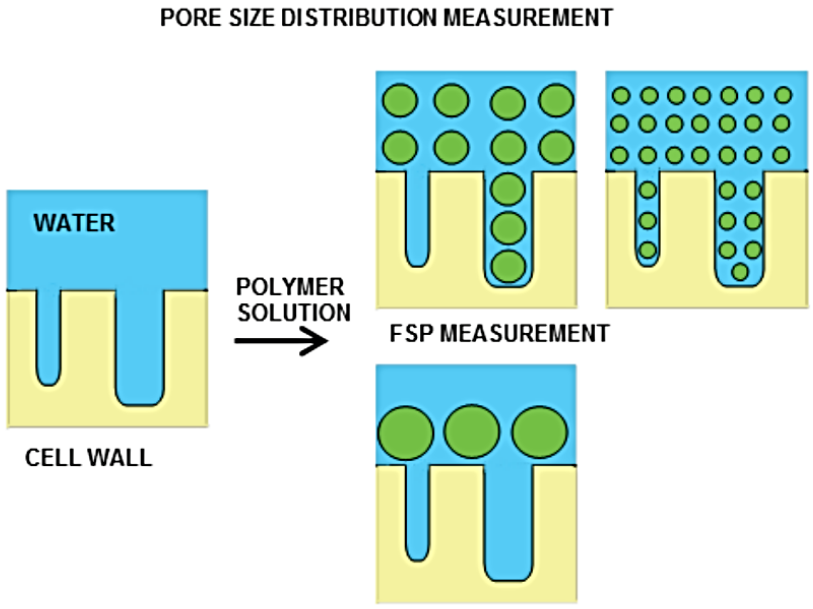

Figure 11: The basics of solute exclusion method (Pönni, Vuorinen et al. 2012a)

Based on this principle, FSP and pore size distribution can be measured using different sizes of probe polymer molecules. A 2×10^6 Da dextran is commonly used to measure fiber saturation points, because the large molecular size (diameter 54 nm) prevents its access into the cell wall pores. However, this Dextran is too large to allow the estimation of the micropores. Hence, the micropore volume is calculated using 2×10^3 Da dextran whose diameter measures 3.2 nm (Lovikka, Khanjani et al. 2016).

The fiber saturation point is calculated using following equation:

$$FSP = \frac{w+q}{p}\left\{1 - \left(\frac{w}{w+q}\right)\left(\frac{C_i}{C_f}\right)\right\} \quad (29)$$

Here, p is the dry weight of fiber [g] q is the amount of water [g], w is the weight of dextran solution [g], and C_i and C_f are the initial and final concentration of the solution, respectively. The unit of FSP is g/g, which expresses grams of water per grams of fiber (Pönni, Vuorinen et al. 2012b, Grönqvist, Hakala et al. 2014).

2.4.6. Nuclear Magnetic Resonance (NMR) Cryoporometry

NMR cryoporometry is another pore size distribution measurement method, which is generally applied to different porous samples including silica gels and wood fibers (Viel, Capitani et al. 2004, Webber, Strange et al. 2001). As the TPM method, this method considers the melting/freezing point depression of a liquid confined into a pore according to the Gibbs-Thomson equation (Mitchell, Webber et al. 2008b). For this measurement, typical probes are water or organic solvents, such as cyclohexane (Valiullin 2014). Most commonly, NMR cryoporometry experiments uses ^{1}H NMR, because water and organic probes contain proton in the structure (Mitchell, Webber et al. 2008a).

^{1}H NMR is used to detect the number of proton spins in the liquid as a result of the applied magnetization. The result is a spin-echo signal (Carr, Purcell 1954, Hahn 1950). The spin-echo pulse sequence is selected from within a certain echo time. Spin-echo NMR signal is obtained for the mobile electrons, which magnetization do not relax to zero.

During the first phase of NMR cryoporometry measurement, the samples are cooled, and the liquid in the pores freeze. In this state, no spin-echo NMR signal is obtained, because the magnetization relaxes to zero for the nuclei of immobilize molecule. Then, the temperature is increased in steps, and a new spin-echo NMR experiment is performed in each step. The intensity of the spin echo signal increases with the increase in temperature, and the signal is proportional to the liquid volume. Pore size distribution is obtained by the signal intensity curve related to the temperature (Gane, Ridgway et al. 2004).

2.5. Preparation of well-preserved dry fiber

Well-preserved dry fiber is essential for both N_2 sorption and Hg porosimetry. Despite common, oven-drying or air-drying result in fiber shrinkage. Drying process leads to the evaporation of water from the fiber surface first. Capillary force arises due to the surface tension (surface tension of water is 72.75 mN/m at 20℃). When the capillary force reaches the maximum value, vapor diffusion starts. At a certain point, the rate of water removal from the internal structure becomes smaller than the diffusion rate. The combined effect of capillary and diffusion forces brings the fibrils closer. Stronger hydrogen bond form between the fibers, and thus aggregation and pore collapse (Peng, Gardner et al. 2012).

To avoid such undesired effects, porosimetric analyses substituted oven- and air-drying with three alternative drying methods: freeze-drying (FD), solvent evaporation, and critical point drying (CPD).

2.5.1. Freeze-drying Method

Freeze drying requires two operational stages: freezing using refrigeration and drying in low pressure. During the freezing, ice crystals are formed. Then, drying is carried out in two steps: primary drying and secondary drying. During the primary drying, frozen water sublimes. Then, the non-freezing water is eliminated from the fiber by heating under vacuum during the secondary drying step (Peng, Gardner et al. 2012, Bruttini, Crosser et al. 2001).

Throughout freezing, phase separation from liquid to solid occurs and ice crystal formation during "relatively lower freezing process" might cause shrinkage in fibers (Jin, Nishiyama et al. 2004).

2.5.2. Drying by Solvent evaporation

Fibers can be dried by the evaporation of organic solvent such as ethanol, propanol etc. Solvent evaporation is performed at room temperature. Capillary pressure arises during solvent evaporation due to the difference in surface tension between air and the solvent. This causes fiber shrinkage following same mechanism of air-drying. However, the capillary pressure can be reduced by addition of surfactant (Pierre, Pajonk 2002).

2.5.3. Critical point drying (CPD)

During critical point drying, the sample is dried by liquid evaporation at its critical point (Figure 12). The critical point is a combination of certain pressure and temperature at which the gas phase and the liquid phase of the substance are in equilibrium state. Hence, the phase separation does not exist, because there is no difference in density and surface tension (Kay 1968).

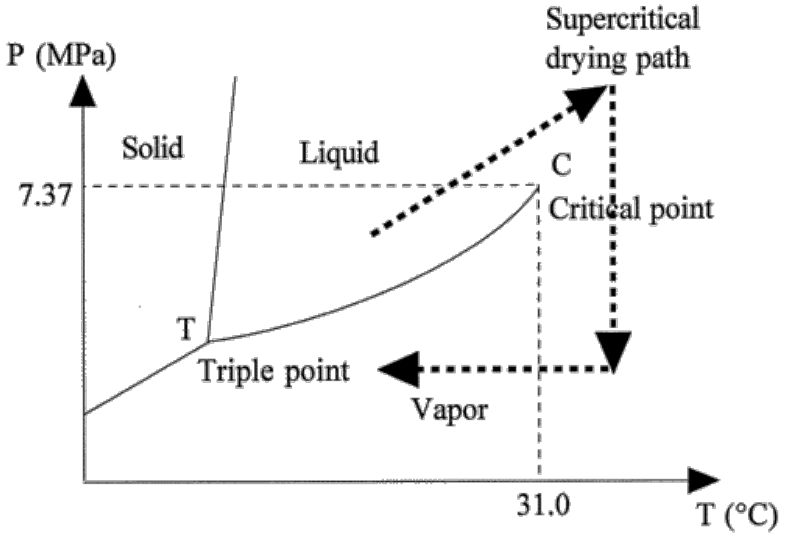

Figure 12: Schematic representation of the supercritical drying process (Pierre, Pajonk 2002).

Biological samples cannot be dried using the critical point of water (374°C and 226 atm), because high temperature and pressure would destroy the samples (Pandithage 2012). However, this problem can be overcome by using a transitional solvent with a suitable critical point. The most common transitional solvent is CO_2, due its availability, environmental friendliness, cost-effectiveness in accordance with having reasonable critical temperature (31°C) and pressure (72.9 atm) (Pandithage 2012).

Before the CPD, samples are exposed to solvent exchange to better preserve the swollen state of the fibers. Water is replaced by fluids such as ethanol and acetone, which are

miscible in both CO_2 and water (Bray 2000). Fibers dried with low-density solvents can preserve their porosity better than those dried with water, because of the lower pressure during consolidation (Henriksson, Berglund et al. 2008).

3. INTRODUCTION TO THE EXPERIMENTAL PART

3.1 Objectives

This thesis work aimed at continued development and diversifying the applications of thermoporosimetry method. The thesis work had two primary objectives:

I. Calculating 'corrected' Gibbs-Thomson coefficient for cellulose-cyclohexane system.

II. Developing a novel platform for quantifying cell wall macropores.

3.2 Hypotheses

This thesis work was designed and executed based on the following hypotheses:

I. Instead of silica or glass as a reference material, the usage of cellulosic materials for determining Gibbs-Thomson coefficient could lead to the more accurate quantitation of pulp PSD. N_2 or Hg porosimetry-based measurements of PSD of CPD-dried pulps might be used to calculate Gibbs-Thomson coefficient using cyclohexane thermoporosimetry. Subsequently, the calculated Gibbs-Thomson coefficient would measure the PSD of pulps in Chex-saturated state. Thus, thermoporosimetry method could reveal the corrected PSD of pulps in wet-state.

II. Pulp contains some macropores which are not accounted in all porosity measurement methods. The combination of Chex-RV and thermoporosimetry would estimate the amount of unaccounted macropores.

At first, the fundamental properties of pulp samples were characterized. Then, pulp porosity in both water-saturated and solvent-saturated state was analyzed to investigate the effect of solvent exchange. The pore size distributions of the CPD dried pulp samples were measured using N_2 and Hg porosimetry. Finally, the Gibbs-Thomson coefficients were calculated by thermoporosimetry using the pore size distribution of dry pulps and the new Gibbs-Thomson coefficients were used to present the PSD of pulps in cyclohexane. Additionally, by combining thermoporosimetry and centrifugation method, cell wall macropores were quantified.

4. MATERIALS AND METHODS

4.1 Materials

This study used five different types of softwood and hardwood pulp samples (Table 2). While hardwood samples were birch hardwood, softwood pulps were mostly a mixture of spruce and pine.

Table 2: List of the sample types, treatments and their suppliers.

Type of Pulp	Sample name	Description	Supplier
Kraft	USW-k-ND	Softwood ;unbleached ;never dried	Stora Enso
	USW-k-D	Softwood; unbleached; machine dried	Stora Enso
	TEMPO	Hardwood; bleached; TEMPO-oxidized	UPM
	BHW-k-ND	Hardwood; bleached; never dried	UPM
Dissolving	BHW-d-D	Hardwood; pre-hydrolyzed; machine dried	Stora Enso

Solute exclusion measurements were performed using dextran T5 and T2000 (Pharmaosmos A/S). Pulp solvent exchanges were carried out using acetone (WVR International; purity ~99.8%) and cyclohexane (Sigma Aldrich; purity ~99.8%). Carbon dioxide (Oy Aga AB; 99.8%) was used for critical point drying.

4.2 Methods

The pulp samples were characterized by fiber dimension measurement, carbohydrate analysis, conductometric titration, water retention value, cyclohexane retention value

(ChexRV), N_2 sorption, thermoporosimetry, Hg-porosimetry, and scanning electron microscopy.

4.2.1 Pulp preparation

The charged groups of the all the pulps were adjusted to Na^+. The pulps were adjusted to 1% concentration with deionized water. The pH of the pulp suspensions was adjusted to 3-3.5 by addition of HCl and stirred for 15 min using magnetic stirrer. Afterwards, the pulps were washed repeatedly with deionized water to remove excess acid. The washing continued until the conductivity of the filtrate decreased below 5 µS/cm. Then, the washed pulps were newly diluted to 1%, and their pH was adjusted to 9-9.5 by addition of NaOH. Finally, the pulp suspensions were stirred for additional 15 min, and the alkaline excess removed through repeated washing until the final conductivity of ca. 5 µS/cm.

4.2.2 Fiber properties

Fiber length, width and fine contents were measured using KajaaniFiberLab^{TM} analyzer developed by Metso Automation. At first, the pulp sample (0.2-0.3 g) was diluted in 5 L deionized water. Then, 50 ml diluted fiber suspension was passed through a capillary system, where a CCD camera took images of the fibers and a laser sensor measured them.

4.2.3 Polysaccharide analysis

The carbohydrate content of the pulps was determined according to the NREL/TP-510-42618 (Sluiter, Hames et al. 2008). At first, 300 mg (bone-dried) of pulp sample was

placed in a test tube with 3 ml 72% H_2SO_4. Then, the sample was hydrolyzed by acid in a water bath incubator at 30℃ for 60 min. After the hydrolysis, the sample was placed in an autoclave bottle, and 84 ml of deionized water was added to dilute the acid to a concentration of 4%. Then, after a careful mixing, it followed a second hydrolysis (60 min at 121℃) in autoclave. Completed the final hydrolysis, the sample was filtered using filtering crucibles, and the filtrate was collected in storage bottles. The sample was placed into an auto-sampler vial through a 0.2 μm filter. The dilution factor of the samples for HPLC was 100. To conclude, the polysaccharide content of the filtrate was measured using a high performance anion exchange liquid chromatography (HPLC) with pulse amperometric detection (HPAEC-PAD) in a Dionex ICS-3000 system. The carbohydrate content was calculated using the data obtained from HPLC.

4.2.4 Conductometric titration

The charge properties of the pulp samples were measured by conductometric titration according to SCAN-CM 65:02 standard. In this process, the acid groups of pulp samples were converted to H^+ form and titrated with sodium hydroxide. At first, 3-5 g (bone dry basis) of pulp were suspended in 0.001 M HCl solution (pH ~2) for 15 min. Then, the suspension was filtered, and the acid in excess was removed washing the sample with deionized water. The washing was performed repeatedly until the conductivity of the filtrate reached value below 5 μS/cm. Afterwards, about 1 g (bone dry basis) pulp was placed into a 600 ml beaker, followed by the addition of 490 ml CO_2-free distilled water and 10 ml of 0.05 M NaCl. Titration was performed using a Metrohm 751 GPD Titrino equipped with Tiamo1.2.1 software. After the titration, the pulp suspension was filtered onto a pre-weighed filter paper and oven dried at 105℃ for at least 4 hours in order to

measure the exact dry matter content of pulp. Finally, the total acidic group content was measured by equation.

$$X = \frac{C_t.\ v_2}{m} \quad (30)$$

Here, X is the total content of acidic group; m is the dry mass of the pulp; C_t and V_2 are the concentration NaOH in µmol/l and volume of NaOH in liter consumed at the second intersection point, respectively.

4.2.5 Water retention value (WRV)

WRV measurements were performed according to the ISO 23714:2007 standard. At first, the consistency of the pulp was adjusted to 10-13%. Then, for each sample, 1.54±0.1 g (oven dry basis) pulp was uniformly distributed on the top of a wire mesh screen (aperture: 125 µm) and centrifuged (at 3000xg for 15 min) as per SCAN-C 102 XE method. Immediately after the centrifugation, the resulting pulp pad was weighted and oven-dried at 105°C for min. 4 hours. Finally, its dry mass was recorded, and the water retention value was calculated using the equation:

$$WRV = \frac{M_W - M_d}{M_d} \quad (31)$$

Where, M_w and M_d are the mass of the sample after the centrifugation and the oven drying, respectively.

4.2.6 Solute exclusion method for fiber saturation point

Fiber saturation point (FSP) is measured by solute exclusion. This measurement considers the inaccessibility of a water-soluble probe molecule, which have larger size compared to the pore size of the cell wall.

At first, 0.7 g (bone-dry) pulp was mixed with 35 ml of 2% dextran solution in a disposable centrifuge tube. Mixing was maintained for 60 min using a rotational mixture Heidolph REAX2. The resulting mixture was centrifuged for 10 min at 3500 g. Then, 20 ml of dextran solution was extracted using a syringe without perturbing the centrifuged fiber layer. Afterwards, 10 ml of extracted dextran solution was inserted into a polarimeter tube. The polarimeter measured the concentration of the dextran solution in form of optical rotation. The optical rotation was calculated by an Autopol IV polarimeter at a wavelength of 436 nm. After the measurement, the pulp was washed thoroughly with deionized water to remove the dextrans. Finally, the accurate dry weight of pulp was measured, and the fiber saturation point was calculated using equation

$$FSP = \frac{W_{dex}+W_{water}}{W_{dried}} - \frac{W_{dex}}{W_{dried}} \times \frac{\alpha_i}{\alpha_f} \quad (32)$$

Where W_{dex} , W_{water} and W_{dried} are respectively the masses of the dextran solution, the pulp water and the bone dry pulp. On the other hand, α_i and α_f are the optical rotation of the dextran before and after addition to pulp.

4.2.7 Solvent exchange and critical point drying

Solvent exchange was carried out according to a revised version of Lovikka's method (Lovikka, Khanjani et al. 2016). At first, the pulps were carefully rinsed with fresh

acetone. Solvent exchange was performed seven times, and zeolite was placed into the sample bottle to adsorb moisture after final washing. The acetone-saturated samples were placed in a dialysis membrane tube with a molecular weight cut-off value of 50000 dalton. The samples were further dialyzed in acetone for additional 24 hours. During dialysis, the solvent was changed twice, and the system was stirred steadily with magnetic stirrer.

On the other hand, the solvent exchange from water-acetone-cyclohexane was done according to above-mentioned processes, but without using the dialysis membrane. The acetone-exchanged samples were further washed with cyclohexane seven times. Finally, zeolite was placed into cyclohexane exchanged sample bottle.

During CPD drying, the acetone-exchanged pulps were dried using a Leica EM CPD300 critical point drier. Acetone was exchanged with CO_2 with more than 25 cycles for 60 min followed by removal of CO_2 for 30 min. The supercritical state of CO_2 was reached by heating the sample at 35℃ under 75 bar.

4.2.8 Differential Scanning Calorimetry

The thermoporosimetric measurements were performed with a Mettler 821e Differential Scanning Calorimeter (DSC). The instrument was calibrated using distilled water and 99.99% pure mercury. A step program with 0.02℃ and 10 min isothermal step were used for calibration. The calibration sample measured ca. 2 mg water and 20-30 mg mercury, respectively at a temperature of 0.00℃ and -38.88℃. Heat calibration was performed by melting water and mercury at a constant 5℃/min heating rate. Latent heat (H_m) of water

and mercury were 335.98 J/g and 11.4 J/g, respectively. The temperature accuracy of the intercooler was ±0.04°C, while the heat accuracy was approximately 1-2%.

Cyclohexane-saturated pulp samples were placed into an aluminum pan. Cyclohexane content was adjusted to 2-3 g chex/g solids, and the pan was sealed with a lid. After the measurement, the samples were weighed again to ensure no leaking had occurred. Then, the lid was punched to make a small hole, and the sample was dried in the oven at 105°C. The drying was continued for at least 4 hours for measuring the dry matter content of the pulp. The reproducibility was checked by analyzing at least 3 replicates for each pulp.

The pore volume and PSDs of the pulps was measured using an isothermal step method (Figure 13).

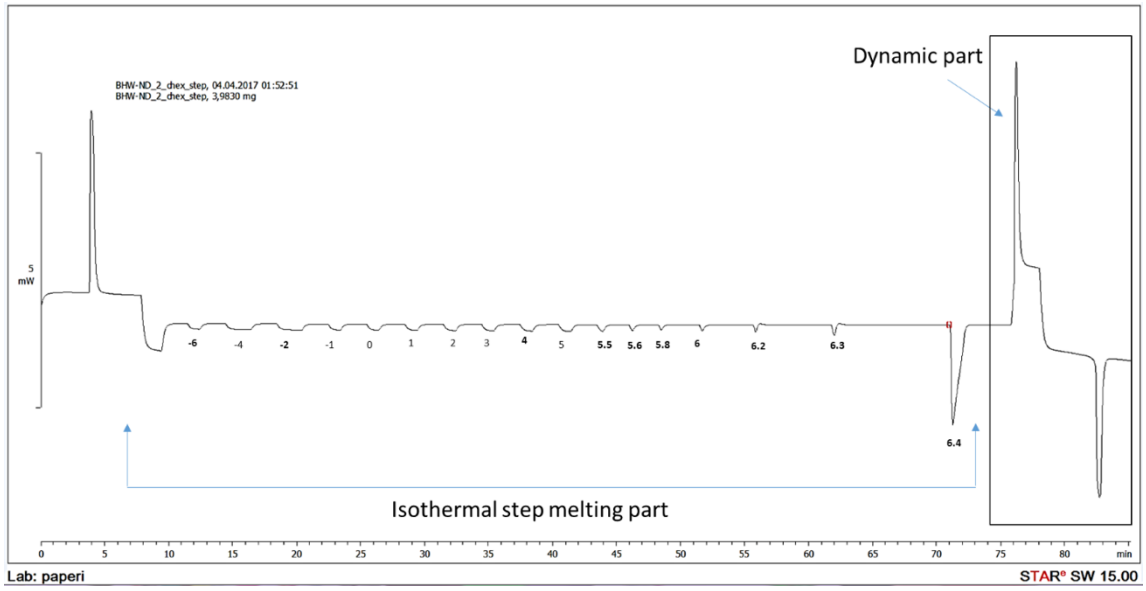

Figure 13: An example of step melting curve used to calculate pore size distribution.

Initially, the sample was frozen lowering its temperature to -15°C. Then, the frozen cyclohexane was melted in steps. The non-linear temperature steps occurred at –6.0, –4.0, –2.0, –1.0, 0.0, 1.0, 2.0, 3.0, 4.0, 5.0, 5.5, 5.8, 6.0, 6.2, and 6.3℃.

In each step, the temperature was kept constant until melting was completed. At each temperature, the specific heat was calculated by integrating the endothermic peaks. The latent heats from each step were used to calculate the amount of melted cyclohexane. The latent heat H_L was calculated using equation (24). Finally, the pore volume was calculated by converting H_L by the equation (25).

The amount of non-freezing cyclohexene (NFC) was calculated by subtracting the freezing cyclohexane from the total cyclohexane content of the sample. Additionally, bulk cyclohexane fraction was measured by subtracting freezing bound chex and NFC from the total pore volume of ChexRV values.

4.2.9 N_2 sorption measurement

Nitrogen adsorption analyzer Micromeritics Tristar II measured pulp BET specific surface area, pore volume, and pore size distribution. The device was calibrated using silica-alumina reference material before performing the measurement. For each sample, the isotherms were achieved by the analysis of around 0.1 g dry sample. Then, Micromeritics Tristar 3020 analyzed the isotherms to calculate specific surface area and pore volume based on the BET equation, while pore size distribution according to the Barrett-Joyner-Halenda (BJH) method. The samples were reweighed after the measurement, and the weight was reduced 2-3%. The repeatability of the results was controlled by multiple parallel measurements.

4.2.10 Mercury porosimetry

Mercury porosimetry experiment was performed in Åbo Akademi, Turku. The measurements were carried out using a Pascal 140/440 instrument (Thermo Fisher Scientific Inc., GER). Intrusion and extrusion measurements were carried out over a pressure range of 0.15-400 MPa. The pressure increase speed was 6-19 MPa min^{-1}, whereas the pressure decrease speed was 8-35 MPa min^{-1}. The surface tension of mercury was 0.48 N/m and the contact angle was 140^{o}. Finally, the instrument calculated the pore size distribution using the Laplace equation. The samples were measured after 7 days of CPD drying.

4.2.11 Gibbs-Thomson coefficient from Hg-porosimetry and thermoporosimetry

A mathematical correlation was established between the incremental pore volumes obtained from Hg porosimetry and the diameter of the pore with the cumulative pore volumes obtained from thermoporosimetry. Based on this correlation, new diameters were obtained for each thermoporosimetry-based incremental pore volume. According the Gibbs Thomson equation (1), the new diameter D was plotted against the $1/\Delta T$, and a new Gibbs Thomson co-efficient was obtained from the slope.

4.2.12 Imaging

Optical microscopy was used to observe the morphology of wet TEMPO fibers both in water and acetone. The images were taken using a Leica ICC50 HD optical microscope. On the other hand, scanning electron microscopy (SEM) was used to examine the morphology of the fibers. CPD dried samples were placed carefully in the sample holder to avoid the moisture exposures of samples. Any compression was avoided to prevent the surface collapse. The samples were sputtered with gold for 90 seconds at 20 mA. The images were taken using a Sigma VP (Zeiss) connected to a secondary electron detector with an acceleration voltage of 1.2-1.5 keV.

5. RESULTS AND DISCUSSIONS

5.1 Characterization of fibers

Physical properties such as fiber length, width, fine content and chemical composition such as polysaccharide content can modulate the fiber pore size. Therefore, the characterization of pulp was considered necessary.

5.1.1 Measurement of fiber length, width and fine content

Softwood fibers are longer and wider than hardwood fibers. Consistent with literature values, it was found that average length and width of the hardwood fibers were shorter than the softwood fibers (length 1.4-1.8 mm and width 28-30 μm). The dissolving pulps were the shortest (0.6-0.8 mm) and the thinnest (~17 μm) fibers among all the pulp samples

Figure 14). The width (18-19 μm) of hardwood TEMPO fibers was similar to that of the hardwood never dried fibers (~20 μm) (Figure 14). However, the fiber lengths of TEMPO-oxidized fibers were similar to the softwood fibers (Figure 14).

Several components, such as ray cells, axial parenchyma cells, and fiber fragments originating from chipping, cooking and bleaching constitute the fine content of the chemical pulps (Meyers, Nanko 2005). On average, the pulps had no more than 1.60% fine content suggesting the good integrity of the fibers (Figure 14).

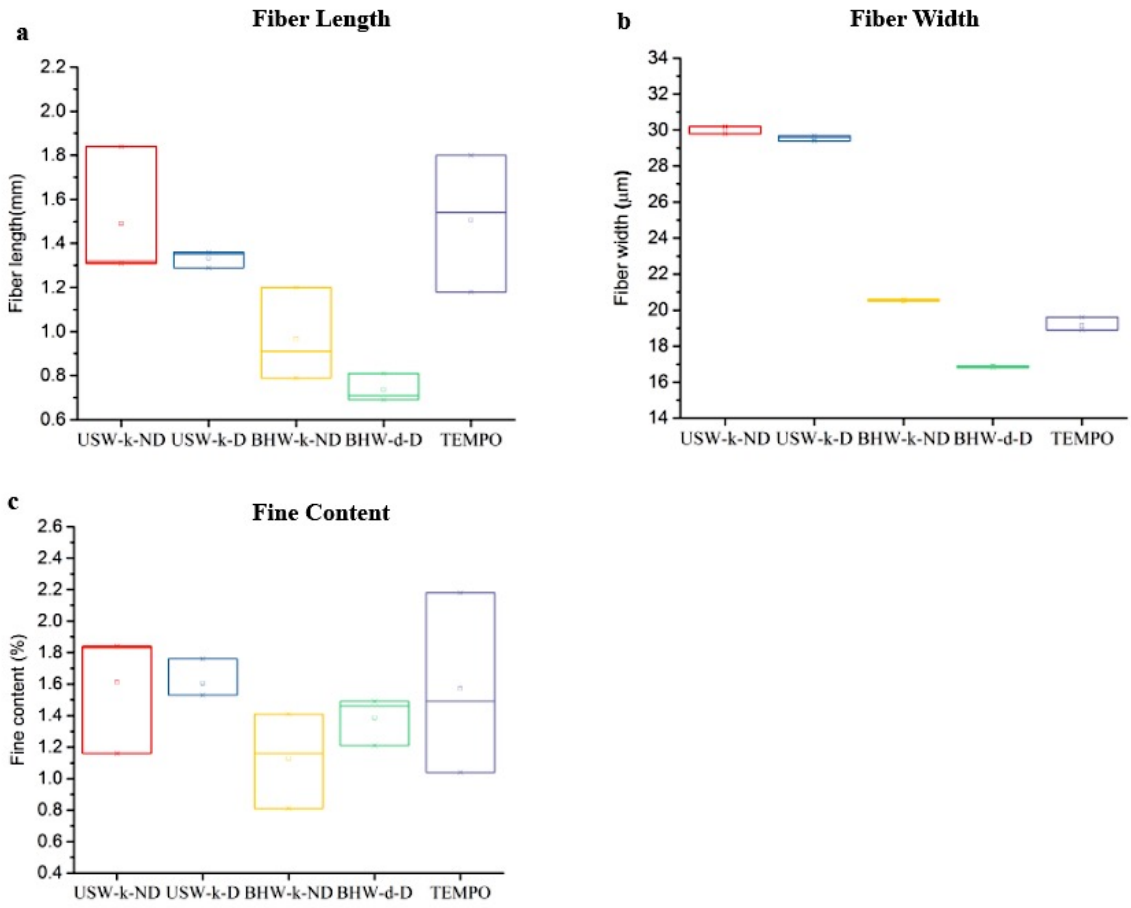

Figure 14: Comparison of fiber length (a), width (b) and the fine contents(c) of different types of fiber sample

5.1.2 Polysaccharide content

Plant cell wall microfibrils are naturally interspersed with the lignin and hemicellulose. During the pulping process, lignin and hemicellulose contents are dissolved, creating void volumes in the fiber wall. Although fiber swelling forces arise from the charges, hydrophilic hemicellulose also contributes to the fiber swelling. Fiber swelling opens up the fiber surface area increasing porosity of the fiber. Therefore, overall polysaccharide content can significantly modulate the porosity of the fiber.

According to the results, the hemicellulose content of BHW-K-ND pulp accounted for ~5% more compared to the softwood kraft pulp (Table 3). Softwood fibers contained about 8% galactoglucomannan. However, galactoglucomannan was completely absent from TEMPO pulp and slightly present in birch hardwood never dried and hardwood dissolving dried pulp (Table 3).

In agreement with Sjostrom 2013, arabino-glucuronoxylan was found to be higher in BHW-ND than in softwood pulps (Table 3).

Table 3: Percentages of cellulose and hemicellulose in various kinds of pulps

		USW-K-ND	**USW-K-D**	**BHW-K-ND**	**BHW-d-D**	**TEMPO**
Cellulose		75 %	73 %	72 %	91 %	77 %
Hemice-llulose	Galactoglucomannan	8 %	8 %	0.3 %	0.4 %	0 %
	Arabino-glucuronoxylan	11 %	11 %	24 %	5 %	20 %
	Total	19 %	19 %	24.3 %	5.4 %	20 %

Dissolving pulps were pre-hydrolyzed and chemically treated during pulping, bleaching and purification process. These processes remove the non-cellulosic components. The hardwood dissolving pulp revealed a significant low amount of total hemicellulose (Table 3). The removal of hemicellulose and lignin enhanced the aggregation between the fibrils. Thus, the pore structure collapsed upon drying.

5.2 Acidic group content

All the key components of the cellulosic fibers contain charged groups. In most pulps, weak carboxylic groups are the only acidic group present. These charged groups modulate the interactions between the pulp fibers as well as between the fibers and solvents. In addition, carboxylic groups influence the accessibility of cellulose and degree of swelling (Lindstrom 1982, Scallan, Grignon 1979). Hence, presence of acidic group content was hypothesized to control the fiber porosity. Thus, before characterizing the fiber porosity, acidic group content of all pulp samples were determined (Figure 15).

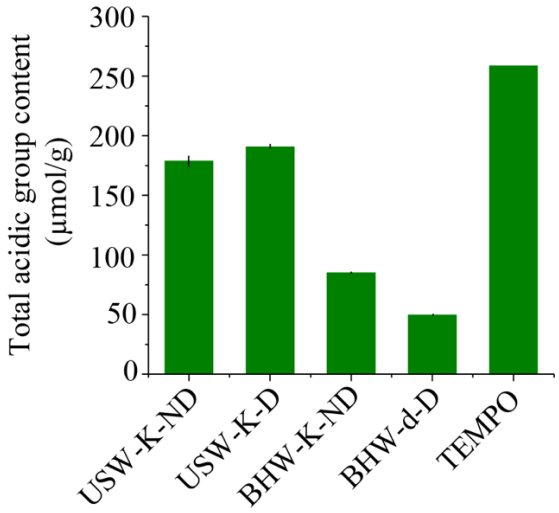

Figure 15: The total acid group contents of softwood and hardwood pulps.

Both softwood pulps presented higher amount of charged groups compared to hardwood never dried pulp. However, TEMPO showed the higher amount of charged groups than any hardwood and softwood pulp. Interestingly, hardwood dissolving pulp contained the least amount of charged groups.

5.3 Water Retention Value and Cyclohexane Retention Value measurement

The water retention value (WRV) of the pulps reflects its ability to take up water and swell. The diffusion of water molecule into the amorphous region of cellulose breaks the inter-molecular hydrogen bonds. As a result, the inter-molecular distance of cellulose chain increases, and this is known as 'fiber swelling' (Akinli-Kocak 2001). Theoretically, more void spaces in the fiber cell wall should retain more water. Thus, WRV correlates positively with the total pore volume (Maloney, Paulapuro 2001, Lovikka, Khanjani et al. 2016).

WRV test was conducted for all softwood and hardwood pulps. Results are reported in Table 4.

Table 4: WRV and ChexRV of the softwood and hardwood pulps

Sample		USW-k-ND	USW-k-D	BHW-k-ND	BHW-d-D	BHW-TEMPO
WRV	mL/g	1.81	1.48	1.70	0.91	4.91
	SD	±0.01	±0.01	±0.00	±0.00	±0.05
ChexRV	mL/g	1.16	0.85	1.28	0.49	1.10
	SD	±0.01	±0.03	±0.00	±0.00	±0.01

Softwood never-dried pulp presented more pore volume than the hardwood never dried pulps. This can be due to the high swelling properties of softwood, because softwood pulp contains more charge groups compared to the BHW-K-ND. Rewetted machine-dried softwood fibers lost about ~20% pore volume. This porosity loss can be the result of

hornification. Hornification is the irreversible compression of fiber during removal of water. Surprisingly, dried dissolving pulp showed the lowest pore volume among all other pulp samples (Table 4). Since BHW-d-D showed the lowest arabino-glucuronoxylan content(Table 3), these fibers were most likely be less resistant to drying and more prone to collapse upon drying.

TEMPO oxidation process introduces carboxylic and aldehyde charged groups into the fibers (Milanovic, Kostic et al. 2012). The addition of these charged groups confer to the pulp a higher degree of accessibility and swelling. Thus, it was hypothesized that existence of high charged groups in the TEMPO fibers would result increased pore volume. Indeed, hardwood TEMPO pulp presented the highest pore volume compared to all hardwood and softwood pulps (Table 4).

ChexRV measurement was performed in order to analyze the pulp swelling behavior in cyclohexane. Although non-polar cyclohexane reduced the pore volume (Table-2), ChexRV can overcome some limitations of the WRV test. Contrary to WRV, the centrifugal force applied during the ChexRV allows to remove the cyclohexane easily from the inter-fiber pores due to the low density of cyclohexane compared to the water. Moreover, the cyclohexane-saturated pulp pad is lighter than water, and the fibers are less swollen. Hence, the centrifugation does not press out cyclohexane from the cell wall (Maloney, Paulapuro 2001).

Unlike the other pulps, TEMPO-oxidized pulp lost about 80% pore volume due to the solvent exchange. The robust change might be due to the absence of charged groups in the non-polar cyclohexane that decrease the swelling effect. As a result, fibers contracted (Figure 16). In addition, the lack of swelling improved the flexibility to the fibers, which

consequentially promoted the aggregation of the fibers and the collapse of the pore structures (Figure 16).

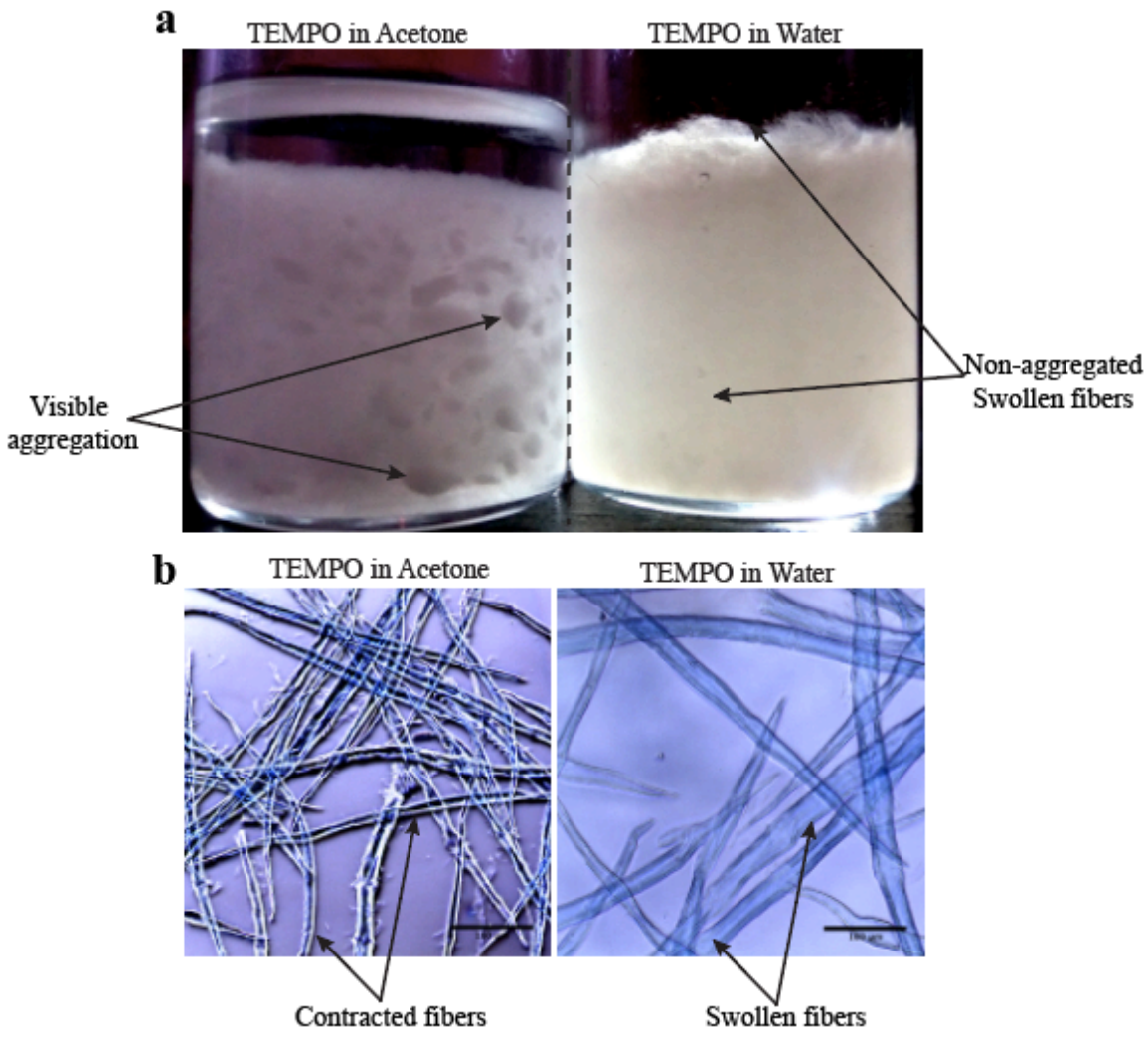

Figure 16: Comparison of the behavior of hardwood TEMPO-oxidized fibers in acetone and water.

5.4 FSP Measurement

Solute exclusion method measures the total amount of water in the cell wall, which is called FSP. Wet pore volume was divided into micro- and mesopores considering the size of the dextran molecules. Solute exclusion data showed lower FSP value for USW-K-D pulp compared to the USW-K-ND. Softwood fiber lost about 20% micropores and 10% mesopores due to hornification (Table 5). As like WRV values, BHW-K-ND showed lower FSP values than the softwood fibers. In addition, dissolving dry pulp (BHW-d-D) reported less degree of mesoporosity.

The microporosity of TEMPO was quite similar to USW-ND. However, TEMPO fiber had significantly higher mesoporosity compared to all other pulps (Table 5). As described in section 5.3, the higher degree of mesoporosity characterizing the TEMPO-oxidized fibers can result from the abundant charged groups.

Table 5: Pore volume measurement from solute exclusion method

Sample	FSP (54 nm)		Micropore (3.2 nm)		Mesopore (3.2-54 nm)	
	mL/g	STD	mL/g	STD	mL/g	STD
USW-k-ND	1.74	±0.03	0.96	±0.01	0.78	±0.04
USW-k-D	1.50	±0.00	0.78	±0.01	0.72	±0.02
BHW-k- ND	1.61	±0.00	0.51	±0.02	1.10	±0.02
BHW-d-D	0.55	±0.02	0.42	±0.00	0.13	±0.02
TEMPO	3.75	±0.04	0.92	±0.00	2.83	±0.04

FSP cannot give information about the macropores (>54nm), because the porosity information of pores larger than 54 nm is absent in FSP. Additionally, the osmotic pressure exerted on the cell wall can squeeze the cell wall pores.

5.5 N_2 sorption

Physisorption isotherms are classified into 6 distinct types as discussed in the section 2.5.2.1. While type IV isotherm represents the adsorption behavior of mesoporous materials, type II isotherm is typical for nonporous or macroporous adsorbent (Figure 10). The area and shape of the hysteresis arises from the specific pore structure. Thus, the pore sizes can be illustrated based on the pattern of the hysteresis loop. According to the results, the hysteresis loops were broader for softwood and never dried hardwood (IV type with H3 hysteresis loop) (Figure 17), which are typical for mesoporous sample.

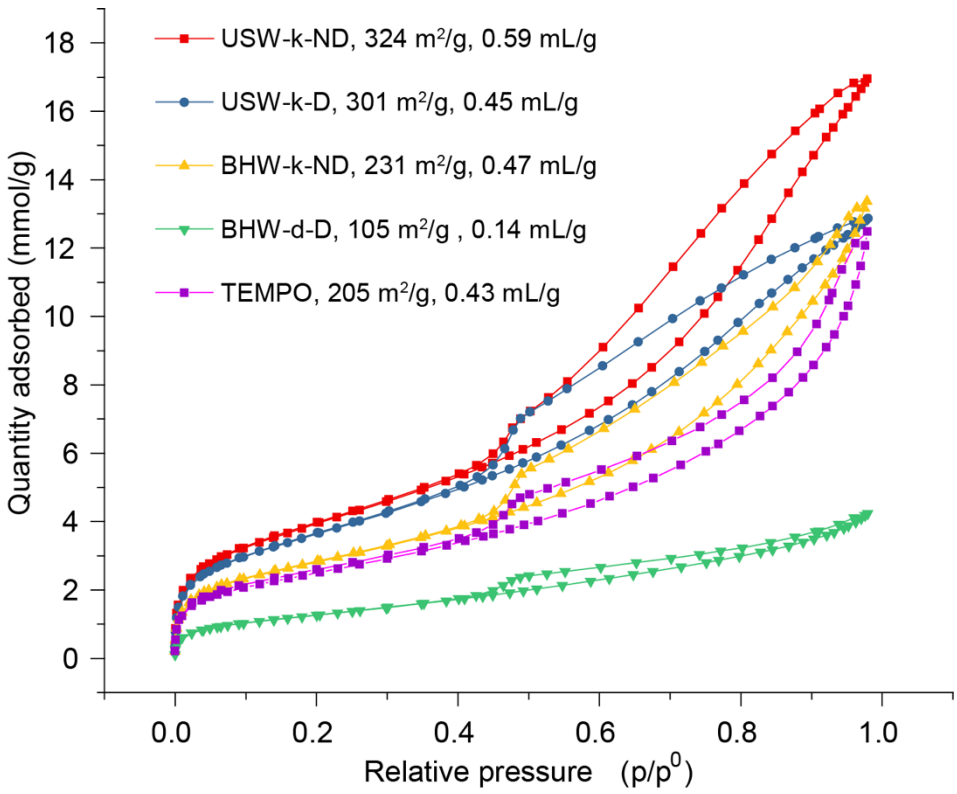

Figure 17: Nitrogen adsorption isotherms of different pulp samples. Surface areas and pore volumes are listed in the legend.

The distance between the adsorption and desorption branch with respect to the volume axis increases with the increase of bottle-neck porosity. This broader hysteresis loop indicated the presence of bottle-neck pore in the fiber or flat ellipse pores (Mistura, Pozzato et al. 2013, Broekhoff 1979).

The adsorption isotherm of the TEMPO-oxidized pulp followed the II type isotherm with H3 hysteresis loop (Figure 17) suggests that TEMPO-oxidized pulp contained higher amount of macropores (Matthias, Katsumi et al. 2015). However, the hysteresis loop of TEMPO-oxidized fibers was narrower than other samples. This could indicate the presence of less bottle-neck pores.

The pore size distribution was interpreted by Barrett-Joyner-Halenda (BJH) method where the adsorption branch of the isotherms was considered only as previously discussed in section 2.5.2.1. The results are illustrated in Figure 18.

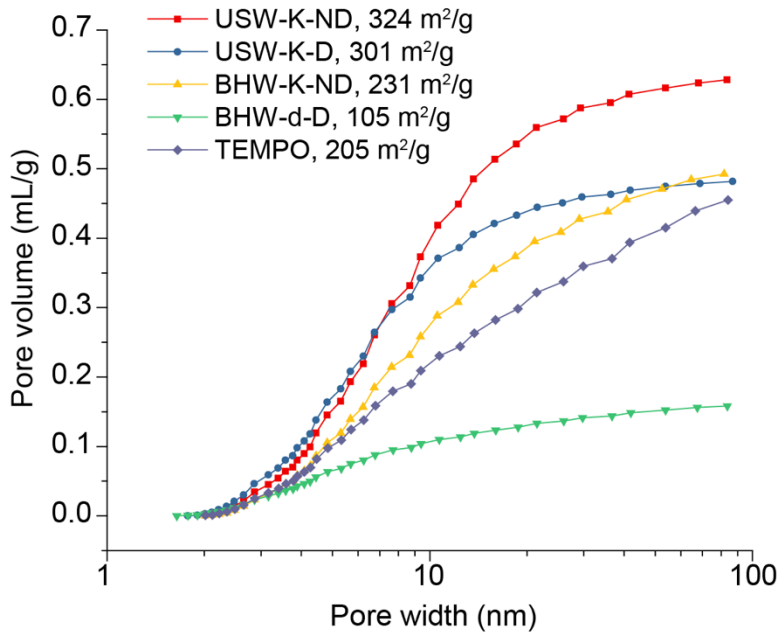

Figure 18: Pore size distributions from N_2 sorption for different softwood and hardwood pulps.

Both softwood pulps showed higher N_2 adsorption compared to hardwood pulps. This suggested that softwood pulps were more porous. Drying process collapsed pore structures as evident from the reduced pore volume of USW-K-D compared to USW-K-ND.

Longer fibers introduce more opened structure, thus a more porous structure (Habibi, Ruiz et al. 2017). Softwood fibers have higher fiber length compared to hardwood fibers

Figure 14). Based on the fiber length, softwood fibers were expected to contain high amount of pores than hardwood fibers. Indeed, nitrogen adsorption isotherms demonstrated the higher porosity of the softwood pulps (Figure 18).

Furthermore, softwood pulp samples revealed more charged groups than hardwood pulp samples. Hypothetically, increased charged groups in the softwood pulps should confer more opened structure and consequently a higher degree of swelling and porosity.

The TEMPO-oxidized pulps reported higher fiber length (Figure 14a), charged groups (Figure 15), FSP (Table 5), WRV and ChexRV values (Table 4). Thus, higher PSD were expected as well. Contrary to this, TEMPO fibers showed a lower PSD (Figure 18). In addition, nitrogen adsorption isotherms suggested the presence of macroporosity (Figure 17).

These paradoxical results might be due to the critical point drying before N_2 sorption, which may have collapsed the pore structures. During solvent exchange before CPD drying, fiber surfaces minimize the increases surface energies by bringing the surfaces closer or by rearrangement of functional groups in the surface (Johansson, Tammelin et al. 2011, Lovikka, Khanjani et al. 2016). This suggests that the pore structures were well-maintained in water, but severely collapsed in solvent as evident from the morphometric

analysis of TEMPO fibers in water and acetone (Figure 16). Nitrogen adsorption isotherm was further validation of decreased PSD of TEMPO in organic solvent.

As expected, BHW-d-D presented lowest PSD compared to all the other kraft pulp samples, which further supported the notion of collapsed pore structures. In N_2 adsorption isotherms, BHW-k-ND and TEMPO did not reach to the plateau (Figure 18) suggesting that BHW-d-D and TEMPO contained higher macropores than USW-K-ND, USW-K-D and BHW-d-D.

5.6 Hg-porosimetry

Hg-porosimetry (detection range: 1-10, 000nm) allows to explore a broader range of PSD, including macropores. The results are reported in Figure 19.

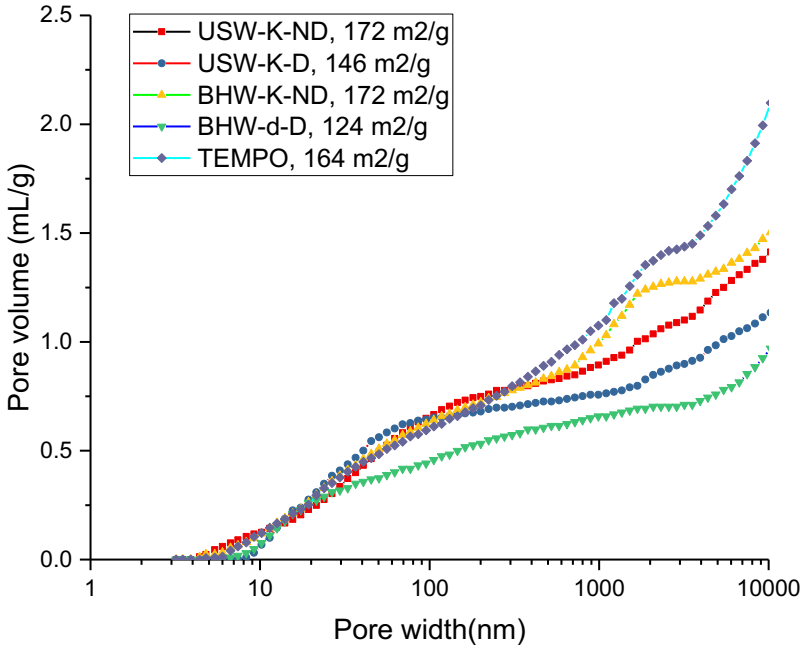

Figure 19: The cumulative pore volumes of the different pulp samples from Hg-porosimetry. The surface areas of the samples are included in the legend.

In mesoporous range, Hg porosimetry showed almost same porosities for all of the pulps except for the BHW-d-D. This might be due to the compression especially in mesopore and micropore range. According to Giesche 2006, as Hg penetrate into the macropores first with the application of pressure during the measurement , the smaller pores (<100 nm) or overlapping pores of soft materials could be affected due to the compression exerted by pressure (Giesche 2006).

In macroporous range, the amount of adsorption followed different pattern than the N_2 sorption. Hg adsorption was highest for TEMPO-oxidized pulp. BHW-K-ND showed higher adsorption than the softwood pulps. Moreover, based on the pattern of N_2-based adsorption isotherms, TEMPO and BHW-K-ND were hypothesized to present more macropores. Indeed, both TEMPO and BHW-K-ND showed a sharp increase of PSD at the macroporous range (50-10000 nm) in Hg-porosimetry (Figure 19). Thus, Hg-porosimetry further confirmed the high abundance of macropores in the TEMPO and BHW-K-ND samples. However, the surface areas of pulp samples were lower than that obtained from N_2 sorption.

5.7 Comparisons of pore volumes

None of the existing methods alone can fully characterize all the available pore types characterizing the pulp samples. In order to produce a credible and comprehensive overview about PSD and to address the weaknesses and strengths of various methods, the results obtained from the different methods were compared.

5.7.1 Comparisons of pore volumes between FSP, ChexRV and N_2 sorption

Figure 20 presented the pore volumes of the pulps in water-saturated state, cyclohexane saturated state and mesopore volumes detected by N_2 sorption. The hypothesis was to use the PSD of mesopore volume from N_2 sorption to calculate Gibbs-Thomson coefficient and later use that coefficient for the PSD calculation in Chex-saturated state. According to previous discussion in section 5.3, during solvent exchange to cyclohexane pore volume reduced due to loss of hydration force and osmotic pressure. Hence, the pore volumes of pulps were decreased in Chex-saturated state.

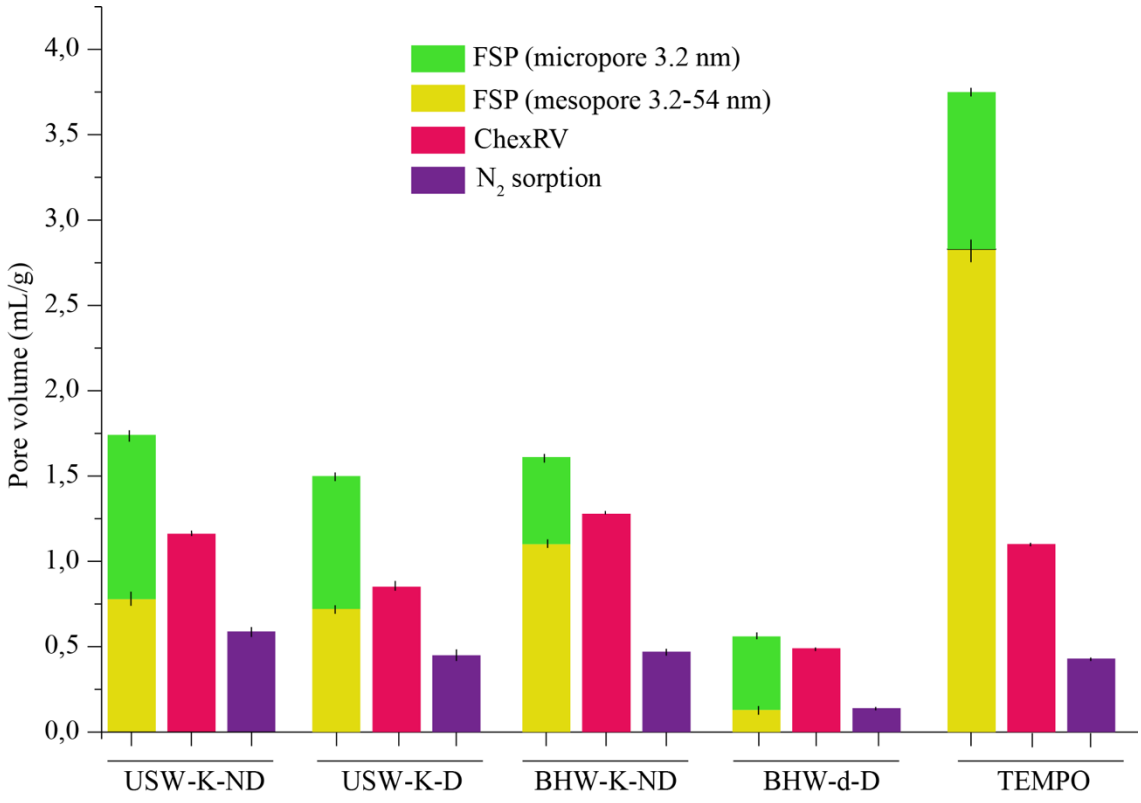

Figure 20: Comparison of the pore volumes measured with FSP, ChexRV and N_2 sorption.

Surprisingly, TEMPO-oxidized pulp showed a huge reduction in pore volume from 3.75 mL/g to 1.10 mL/g due to absence of charge group effect. The pore volumes of CPD dried

pulps from N_2 sorption method presented the pore volumes within mesopore size range. Hence, Gibbs-Thomson coefficient calculated from this limited range of porosity can be used to reveal the broader PSD range in Chex-saturated state. It was expected that the mesopore volume of CPD dried fiber would correlate with the mesopore volume from wet state in water. However, the result showed disagreement with the hypothesis (Figure 20). Lovikka 2016 explained that microporosity and smaller range of mesoporosity can be affected with the combined effect of solvent exchange and CPD drying.

5.7.2 Comparisons of pore volumes obtained from N_2 sorption, ChexRV and thermoporosimetry

Thermoporosimetry measured the total pore volume which is the sum of the freezing and non-freezing pore volume. The bulk fractions were obtained by subtracting the total volume of non-freezing and freezing fraction from ChexRV pore volume. The pore information from wet fibers (in cyclohexane) and dry fibers (CPD dried fibers) were compared (Figure 21).

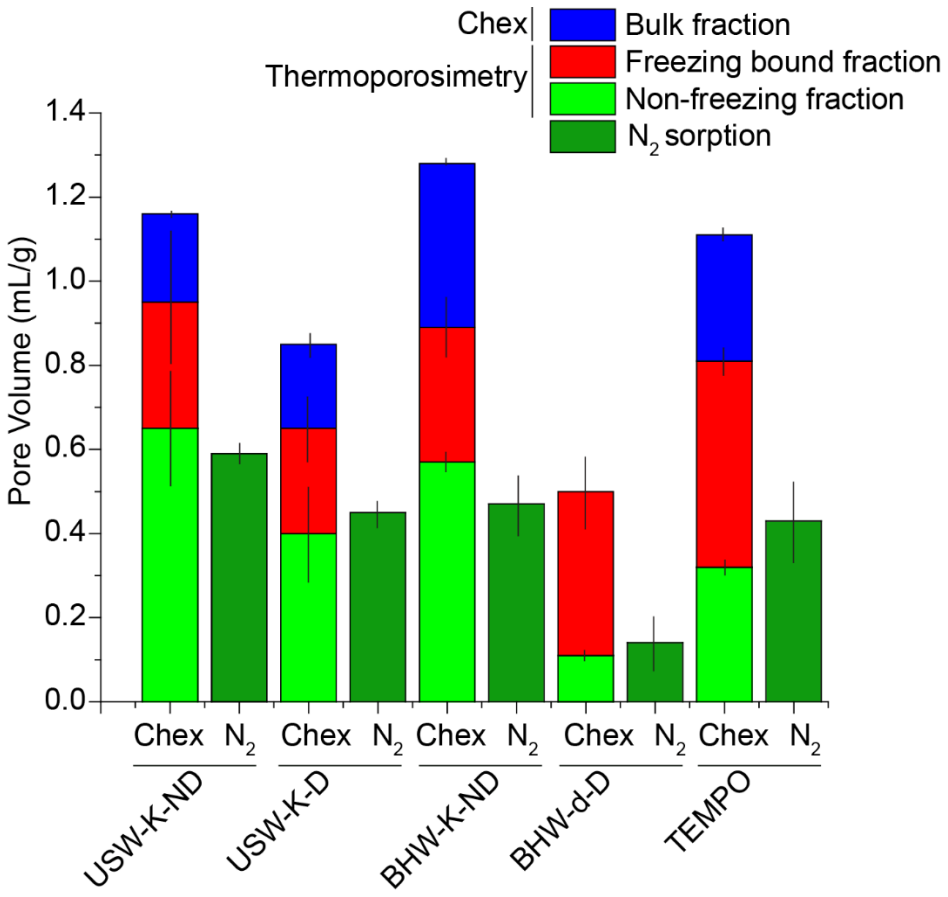

Figure 21: Comparison of total pore volume of pulp samples obtained from thermoporosimetry, N_2 sorption and centrifugation method measurement.

According to TPM measurements, the amount of non-freezing cyclohexane was similar with mesopore volume obtained from N_2 sorption. This suggested that the cyclohexane in both micropores and mesopores did not freeze. It indicated that the PSD from N_2 sorption method could not be used for calculating Gibbs-Thomson coefficient for cyclohexane-cellulose system.

The freezing fraction-cyclohexane pore volumes of pulps mostly obtained from the macropores. Apart from macropores, small pits and inter fiber pores also contributed to the freezing fraction. Considering this situation, inter-fiber pore volumes or overlapping fiber pore volumes were estimated by ChexRV and thermoporosimetric analyses of the pore volume of air-dried fibers (Table-7). Interestingly, both the measurements provided

quite similar inter-fiber pore volume for all the samples. As shown in Table 6, about 0.1-0.2 mL/g pore volume was measured as due to the interference of inter-fiber pores. This overlapping pore volume might introduce some error results either in bulk fraction or in the freezing bound fraction.

Subtraction of this inter-fiber pore volumes from the CPD-dried freezing fraction provided the volume of macropores. The macropore volumes for all the pulps lie between 0.2-0.3 mL/g except TEMPO oxidized pulp, which was significantly high (1.09 mL/g) compared to other pulp samples (Table 6).

Table 6: Contribution of inter-fiber cyclohexane pore volume from both thermoporosimetry and ChexRV measurement.

Sample	Air-dreid pulps			CPD dried pulps	
	Freezing fraction (mL/g)	Nonfreezing fraction (mL/g)	ChexRV (mL/g)	Freezing fraction (mL/g)	Calculated macropore volumes (mL/g)
USW-k-ND	0.18	~0	0.17	0.36	0.18
STD	± 0.02		± 0.00	± 0.05	
USW-k-D	0.13	~0	0.12	0.36	0.23
STD	± 0.00		± 0.00	± 0.08	
BHW-k-ND	0.16	~0	0.11	0.49	0.33
STD	± 0.01		±0.01	± 0.08	
BHW-d-D	0.19	~0	0.11	0.45	0.26
STD	± 0.01		±0.00	± 0.11	
TEMPO	0.08	~0	0.09	1.17	1.09
STD	± 0.02		±0.00	± 0.14	

Table 7 showed the thermoporosimetric analysis of cyclohexane exchanged pulps which were not CPD dried. The non-freezing pore volumes of CPD-dried and non-dried pulps were quite similar. However, the freezing fraction pore volumes of CPD dried pulps were higher than the non-dried pulps. This indicates that non-dried pulps contained more macropores than the calculated volume, which might not be measured with the size range of cyclohexane thermoporosimetry. Moreover, during CPD drying size range macropores might shifted to lower size range due to the shrinkage.

Table 7: Freezing and nonfreezing cyclohexane pore volumes of non-CPD dried and CPD dried pulps obtained from cyclohexane thermoporosimetry

Sample	Solvent exchanged pulps in Chex Thermoporosimetry			CPD dried pulps in Chex Thermoporosimetry		
	Freezing pore volume (mL/g)	non-freezing pore volume (mL/g)	Total pore volume (mL/g)	Freezing pore volume (mL/g)	non-freezing pore volume (mL/g)	Total pore volume (mL/g)
USW-K-ND	0.30	0.65	0.95	0.36	0.66	1.02
STD	±0.16	±0.14		±0.05	±0.14	
USW-K-D	0.25	0.40	0.65	0.36	0.38	0.74
STD	±0.07	±0.11		±0.08	±0.17	
BHW-K-ND	0.32	0.57	0.89	0.49	0.41	0.89
STD	±0.07	±0.07		±0.08	±0.10	
BHW-d-D	0.39	±0.11	0.49	0.45	0.06	0.51
STD	±0.08	0.07		±0.11	±0.20	
TEMPO	0.49	±0.32	0.81	1.17	0.44	1.60
STD	±0.02	±0.09		±0.14	±0.39	

5.7.3 Comparisons of the pore size distributions measured by N_2 sorption and Hg porosimetry

In order to analyze the mesopores, the part of Hg-porosimetric results ranging within 3.5 and 100 nm was compared with the results obtained by N_2 sorption. The non-freezing pore volumes estimated by thermoporosimetry were similar to the pore volumes measured by N_2 sorption (Figure 21). Hence, the pore size distribution of the mesopores was important for calculating the non-freezing layer thickness.

For all the samples, cumulative pore volumes obtained from Hg-porosimetry were lower than those obtained by N_2 sorption (Figure 22). This might be due to the loss of both microporosity and some extent of mesoporosity in Hg-porosimetry. Moisture interference or sample compression during measurement might have contributed to the loss of porosity information. In fact, some compression on the sample was observed during the Hg-porosimetry measurement. Extrusion curve followed the intrusion curves at high pressure, and it was concluded that compression affected pores with a sizes of 30 nm or smaller. This compression might introduce some error for the calculation of non-freezing layer thickness.

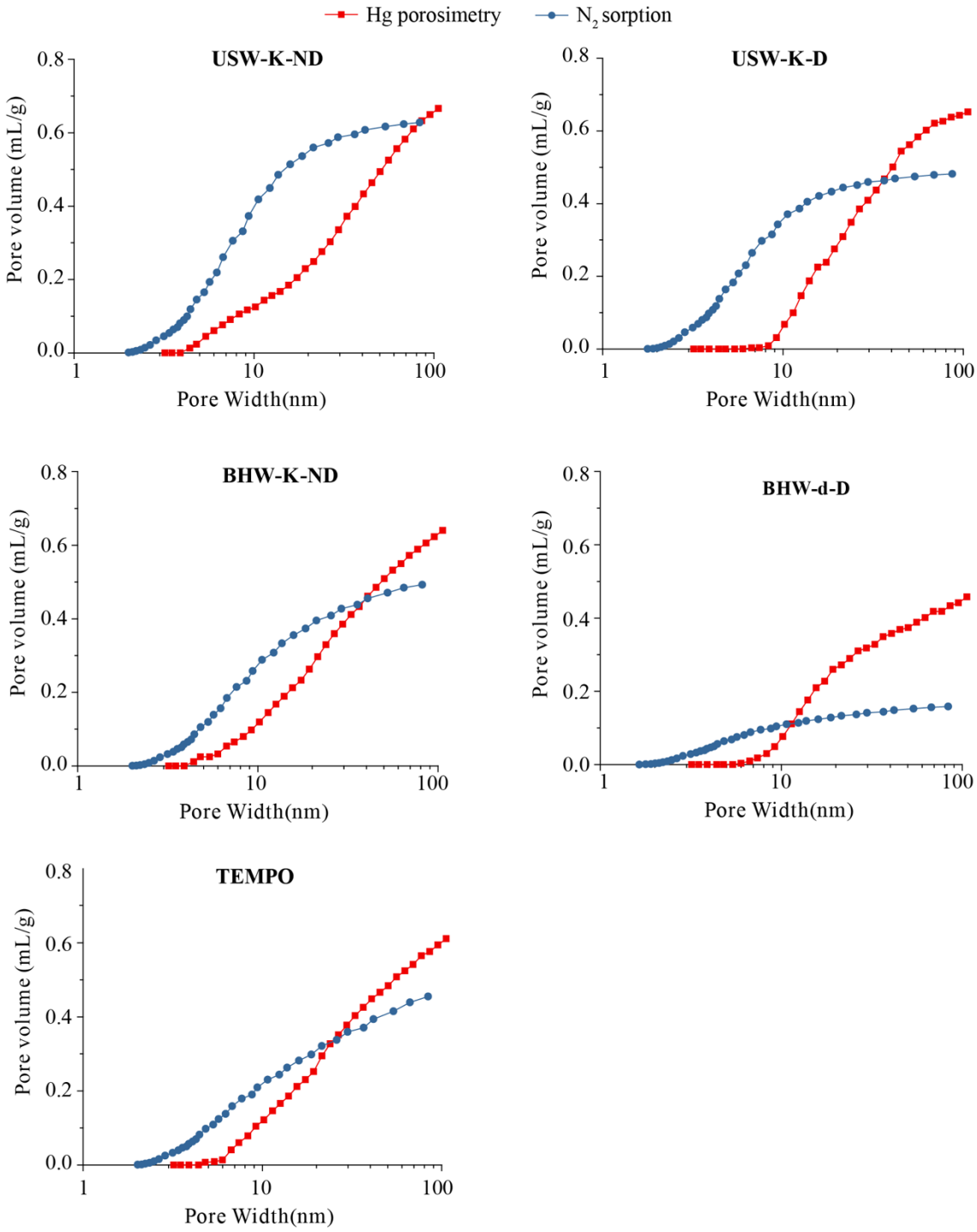

Figure 22: Comparison of pore size distribution between softwood and hardwood samples, obtained from Hg-porosimetry and N_2 sorption.

5.8 Determination of corrected Gibbs-Thomson coefficient

According to previous discussion, PSD of mesoporous volume obtained N_2 sorption was unable to use for calculation of required Gibbs Thomson coefficients for cellulose-cyclohexane system. Because, the freezing fractions of the pulps obtained from the macropores and the cyclohexane in the mesopore did not freeze (Figure 21). Hence, Gibbs Thomson coefficient were calculated for different pulp samples using the PSD of macroporous range from Hg- porosimetry. The values are listed in Table 8.

Table 8: Alternative Gibbs-Thomson coefficients and thicknesses of non-freezing layer.

Sample	Gibbs-Thomson coefficient (nm°C)	Thickness of NFC (nm)
USW-K-ND	159.50	2.04
USW-K-D	28.70	1.26
BHW-K-ND	150.90	1.77
BHW-d-D	11.20	0.57
TEMPO	383.70	2.15

Gibbs-Thomson coefficients were calculated using the pore diameter, where cyclohexane was frozen. This data was acquired by combining thermoporosimetry and Hg-porosimetry (see Appendix I). The Gibbs-Thomson coefficient of USW-K-ND and BHW-K-ND were similar to the coefficient known for cyclohexane in silica having value of 117 nm^0C. However, the coefficients for dry fibers were unreliable. Because, these values resulted PSD at microporous range for the freezing fraction. This was not

consistent as freezing fractions was obtained from macroporous range whereas the cyclohexane in microporous and mesoporous range did not freeze.

Contrary to Hg-porosimetry, mesoporosity data from N_2 sorption was more consistent with the different pore measurement methods (See section 5.7.3). Due to this reason, the thickness of nonfreezing layer was calculated using the surface areas from the N_2 sorption method (Table 8). Nonfreezing thickness values for the pulps are relatively larger than the literature value.

Usually water in the macropores do not freezes due to some kinetic effect or some hydrogen bond interactions or due to the insufficient collection of molecules for crystal formation (see section 2.4.1.3). However, in cyclohexane thermoporosimetry, cyclohexane in both mesopore and micropore did not freeze. Hence, further investigation is required to address the behavior of cyclohexane into the pore. Additionally, Maloney 2001 presented the calculation of surface area contributed by micropores using the nonfreezing micropore volume and the nonfreezing thickness. Cyclohexane thermoporosimetry could not measure that as both mesopore and macropore remained non-frozen.

5.9 Scanning electron micrographs of soft wood and hard wood pulps

Scanning electron microscopy can be used to study the porous structures of pulp samples in nano-scale. In order for fiber morphology analysis, SEM images were obtained from critical point dried softwood and hardwood pulp samples.

Softwood fibers showed well-preserved porosity (Figure 23 a and b). Electron micrograph of USW-K-ND showed higher degree of macropores compared to USW-K-ND, which is in line with the results of the bulk fraction and Hg-porosimetry.

The surface of BHW-k-ND showed uneven pore sizes, which might be due to the presence of high amount of hemicellulose (Table 3). The machine dried dissolving pulp (BHW-d-D) was rewetted and CPD dried. Homogeneous but collapsed dense surface structure was observed (Figure 23 d). This further confirmed the previous findings of low porosity of BHW-d-D pulp samples.

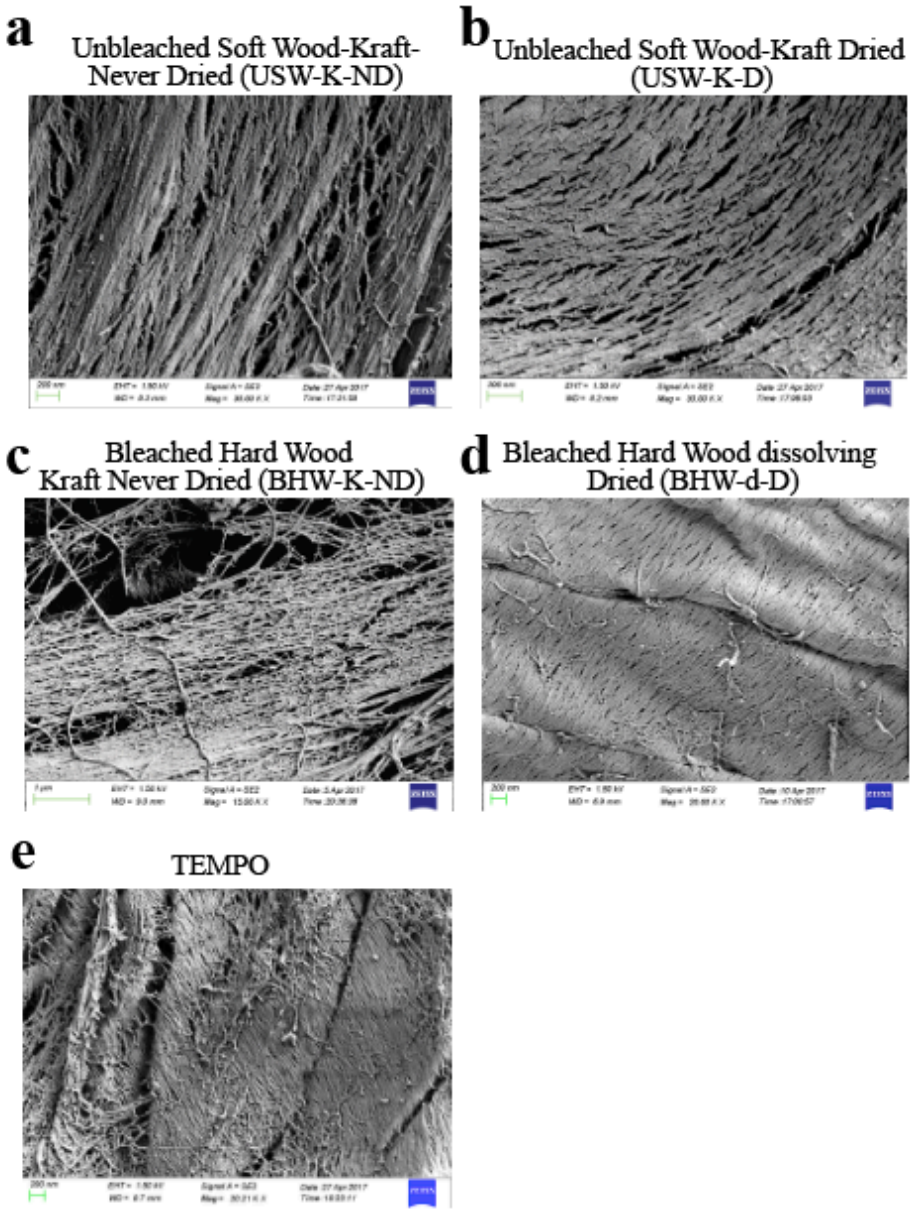

Figure 23: Representative scanning electron micrographs of (a) USW-K-ND, (b) USW-K-D, (c) BHW-K-ND, (d) BHW-d-D and (c) TEMPO-oxidized hardwood.

In agreement with Lovikka et al. (2016), the parallel folded structures of the fiber surface suggested that TEMPO oxidized fibers were originated from Kraft hardwood. Surface rearrangement during solvent exchange might have caused the TEMPO fiber to aggregate. These aggregations were visible in light microscopic images (Figure 16) and SEM images (Figure 23 e). Due to the contraction and aggregation, TEMPO fibers showed reduced pore volume in both cyclohexane and N_2 sorption.

6. CONCLUSIONS

Porous structure of pulp differs according to their origins, preparation processes and compositions. Thus, porous structure is also markedly different between different types of pulps. Considering this variability, Gibbs-Thomson coefficients were hypothesized to be different for different pulp types. Indeed, this study revealed that Gibbs-Thomson coefficients for pulps in cyclohexane thermoporosimetry varied between the pulp types.

Instead of using non-cellulosic material such as silica or glass as reference material, use of cellulosic pulps were hypothesized to be more accurate for deriving Gibbs-Thomson coefficient for PSD determination. This is because heterogeneous porous structure of pulp is vastly different than silica or glass material. To test this hypothesis, a 'corrected' Gibbs-Thomson coefficient was thought to be calculated from PSD obtained from N_2 sorption or Hg porosimetry.

However, non-freezing cyclohexane volume obtained from thermoporosimetry was similar to the pore volumes from N_2 sorption method suggesting the cyclohexane in the mesopores did not freeze. Thus, both in micropore and mesopore range, cyclohexane remained non-frozen in N_2 sorption. Therefore, 'corrected' Gibbs-Thomson coefficient could not be derived from N_2 sorption as freezing pore volume was obtained from macroporous range. Furthermore, due to technical error, 'corrected' Gibbs-Thomson coefficient could not be calculated reliably from Hg porosimetry.

Currently existing methods cannot determine the amount of true macropores in the fiber cell wall. Thus, in this thesis work, combination of Chex-RV and thermporosimetry was hypothesized to provide estimated amount of cell wall macropores. In line with the hypothesis, amount of cell wall macropores for different pulps were calculated from Chex-RV and thermporosimetry.

Finally, this study aimed at further development of the thermoporosimetry method. A framework for determining corrected Gibbs-Thomson coefficient based on cellulosic pulp was presented. However, technical limitations should be overcome in order for calculating reliable and reproducible Gibbs-Thomson coefficient for accurate PSD determination.

In sum, this study set-up a groundwork for overcoming the vital limitations of thermoporosimetry-based pore size distribution of cellulosic pulps. Furthermore, this work demonstrated a unique platform for quantification of macropores in the fiber cell wall.

REFERENCES

AARNE, N., 2013. *Expanding the property space of cellulosic materials with multifunctional polymers*, Doctoral dissertation, Aalto University, Degree Programme in Chemical Technology, Espoo, pp.4-5

AARNE, N., KONTTURI, E. and LAINE, J., 2012. Influence of adsorbed polyelectrolytes on pore size distribution of a water-swollen biomaterial. *Soft Matter,* **8**(17), pp. 4740-4749.

AKINLI-KOCAK, S., 2001. The influence of fiber swelling on paper wetting.

ALLAN, G., BALABAN, C., BELLEFEUILLE-WILLIAMS, C., CARROLL, J., CARROLL, S., DUTKIEWICZ, J., GARNER, B., KO, Y., LEE, A. and MCCONNELL, W., 1991. The microporosity of pulp: a key to new markets. *Tappi journal (USA),* .

ANDREASSON, B., FORSSTRÖM, J. and WÅGBERG, L., 2003. The porous structure of pulp fibres with different yields and its influence on paper strength. *Cellulose,* **10**(2), pp. 111-123.

BARRETT, E.P., JOYNER, L.G. and HALENDA, P.P., 1951. The determination of pore volume and area distributions in porous substances. I. Computations from nitrogen isotherms. *Journal of the American Chemical Society,* **73**(1), pp. 373-380.

BERLIN, E., KLIMAN, P.G. and PALLANSCH, M.J., 1970. *Changes in state of water in proteinaceous systems.*

BERRY, S.L. and RODERICK, M.L., 2005. Plant–water relations and the fibre saturation point. *New Phytologist,* **168**(1), pp. 25-37.

BRAY, D., 2000. Critical Point Drying of Biological Specimens for Scanning Electron Microscopy. In: J.R. WILLIAMS and A.A. CLIFFORD, eds, *Supercritical Fluid Methods and Protocols.* Totowa, NJ: Humana Press, pp. 235-243.

BROEKHOFF, J.C.P., 1979. *Mesopore Determination from Nitrogen Sorption Isotherms: Fundamentals, Scope, Limitations.*

BRUN, M., LALLEMAND, A., QUINSON, J. and EYRAUD, C., 1977. A new method for the simultaneous determination of the size and shape of pores: the thermoporometry. *Thermochimica acta,* **21**(1), pp. 59-88.

BRUTTINI, R., CROSSER, O.K. and LIAPIS, A.I., 2001. EXERGY ANALYSIS FOR THE FREEZING STAGE OF THE FREEZE DRYING PROCESS. *Drying Technology,* **19**(9), pp. 2303-2313.

CARR, H.Y. and PURCELL, E.M., 1954. Effects of Diffusion on Free Precession in Nuclear Magnetic Resonance Experiments. *Physical Review,* **94**(3), pp. 630-638.

CIOLACU, D., PITOL-FILHO, L. and CIOLACU, F., 2012. Studies concerning the accessibility of different allomorphic forms of cellulose. *Cellulose,* **19**(1), pp. 55-68.

DE LANGE, M.F., VLUGT, T.J.H., GASCON, J. and KAPTEIJN, F., 2014. Adsorptive characterization of porous solids: Error analysis guides the way. *Microporous and Mesoporous Materials,* **200**, pp. 199-215.

DEFAY, R., 1966. 1. Prigogine, A. Bellemans and DH Everett. *Surface tension and adsorption,* , pp. 158.

DEFAY, R., PRIGOGINE, I., BELLEMANS, A. and EVERETT, D., 1966. Surface Tension and Absorption, 432 pp.

DEODHAR, S. and LUNER, P., 1980. Measurement of Bound (Nonfreezing) Water by Differential Scanning Calorimetry. *Water in Polymers.* AMERICAN CHEMICAL SOCIETY, pp. 273-286.

DIMIC-MISIC, K., PUISTO, A., GANE, P., NIEMINEN, K., ALAVA, M., PALTAKARI, J. and MALONEY, T., 2013. The role of MFC/NFC swelling in the rheological behavior and dewatering of high consistency furnishes. *Cellulose,* **20**(6), pp. 2847-2861.

EMMETT, P.H. and BRUNAUER, S., 1937. The use of low temperature van der Waals adsorption isotherms in determining the surface area of iron synthetic ammonia catalysts. *Journal of the American Chemical Society,* **59**(8), pp. 1553-1564.

ENDO, A., YAMAMOTO, T., INAGI, Y., IWAKABE, K. and OHMORI, T., 2008a. Characterization of nonfreezable pore water in mesoporous silica by thermoporometry. *The Journal of Physical Chemistry C,* **112**(24), pp. 9034-9039.

ENDO, A., YAMAMOTO, T., INAGI, Y., IWAKABE, K. and OHMORI, T., 2008b. Characterization of Nonfreezable Pore Water in Mesoporous Silica by Thermoporometry. *The Journal of Physical Chemistry C,* **112**(24), pp. 9034-9039.

EYLEY, S. and THIELEMANS, W., 2014. Surface modification of cellulose nanocrystals. *Nanoscale,* **6**(14), pp. 7764-7779.

FAHLÉN, J., 2005. *The cell wall ultrastructure of wood fibres effects of the chemical pulp fibre line.* Stockholm: KTH.

FARID, M.M., KHUDHAIR, A.M., RAZACK, S.A.K. and AL-HALLAJ, S., 2004. *A review on phase change energy storage: materials and applications.*

FENGEL, D. and WEGENER, G., 1983. Structure and Ultrastructure. *Wood: chemistry, ultrastructure, reactions.* Walter de Gruyter, pp. 14.

GALIN, J. and GALIN, M., 1992. Water sorption in poly (ammonium sulfopropylbetaines). II. Sorption isotherms. *Journal of Polymer Science Part B: Polymer Physics,* **30**(10), pp. 1113-1121.

GANE, P.A.C., RIDGWAY, C.J., LEHTINEN, E., VALIULLIN, R., FURÃ³, I., SCHOELKOPF, J., PAULAPURO, H. and DAICIC, J., 2004. Comparison of NMR Cryoporometry, Mercury Intrusion Porosimetry, and DSC Thermoporosimetry in Characterizing Pore Size Distributions of Compressed Finely Ground Calcium Carbonate Structures. *Industrial & Engineering Chemistry Research,* **43**(24), pp. 7920-7927.

GIESCHE, H., 2006. Mercury Porosimetry: A General (Practical) Overview. *Particle & Particle Systems Characterization,* **23**(1), pp. 9-19.

GORING, D., 1977. A speculative picture of the delignification process. ACS Publications, pp. 273-277.

GROEN, J.C., PEFFER, L.A.A. and PÃ©REZ-RAMÃREZ, J., 2003. Pore size determination in modified micro- and mesoporous materials. Pitfalls and limitations in gas adsorption data analysis. *Microporous and Mesoporous Materials,* **60**(1-3), pp. 1-17.

GRÖNQVIST, S., HAKALA, T.K., KAMPPURI, T., VEHVILÄINEN, M., HÄNNINEN, T., LIITIÃ¤, T., MALONEY, T. and SUURNÄKKI, A., 2014. Fibre porosity development of dissolving pulp during mechanical and enzymatic processing. *Cellulose,* **21**(5), pp. 3667-3676.

HABIBI, M., RUIZ, E., LEBRUN, G. and LAPERRIE`RE, L., 2017. Effect of surface density and fiber length on the porosity and permeability of nonwoven flax reinforcement. *Textile Research Journal,* , pp. 0040517517708542.

HAHN, E.L., 1950. Spin Echoes. *Physical Review,* **80**(4), pp. 580-594.

HALLAC, B.B. and RAGAUSKAS, A.J., 2011a. Analyzing cellulose degree of polymerization and its relevancy to cellulosic ethanol. *Biofuels, Bioproducts and Biorefining,* **5**(2), pp. 215-225.

HALLAC, B.B. and RAGAUSKAS, A.J., 2011b. Analyzing cellulose degree of polymerization and its relevancy to cellulosic ethanol. *Biofuels, Bioproducts and Biorefining,* **5**(2), pp. 215-225.

HAUL, R., 1982. S. J. Gregg, K. S. W. Sing: Adsorption, Surface Area and Porosity. 2. Auflage, Academic Press, London 1982. 303 Seiten, Preis: $ 49.50. *Berichte der Bunsengesellschaft für physikalische Chemie,* **86**(10), pp. 957-957.

HAY, J.N. and LAITY, P.R., 2000. *Observations of water migration during thermoporometry studies of cellulose films.*

HENRIKSSON, M., BERGLUND, L.A., ISAKSSON, P., LINDSTRÖM, T. and NISHINO, T., 2008. Cellulose Nanopaper Structures of High Toughness. *Biomacromolecules,* **9**(6), pp. 1579-1585.

ISHIKIRIYAMA, K. and TODOKI, M., 1995. Pore Size Distribution Measurements of Silica Gels by Means of Differential Scanning Calorimetry. *Journal of colloid and interface science,* **171**(1), pp. 103-111.

ISHIKIRIYAMA, K., TODOKI, M., KOBAYASHI, T. and TANZAWA, H., 1995. Pore Size Distribution Measurements of Poly(methyl methacrylate) Hydrogel Membranes for Artificial Kidneys Using Differential Scanning Calorimetry. *Journal of colloid and interface science,* **173**(2), pp. 419-428.

JIN, H., NISHIYAMA, Y., WADA, M. and KUGA, S., 2004. Nanofibrillar cellulose aerogels. *Colloids and Surfaces A: Physicochemical and Engineering Aspects,* **240**(1–3), pp. 63-67.

JOHANSSON, L., TAMMELIN, T., CAMPBELL, J.M., SETÄLÄ, H. and ÖSTERBERG, M., 2011. Experimental evidence on medium driven cellulose surface adaptation demonstrated using nanofibrillated cellulose. *Soft Matter,* **7**(22), pp. 10917-10924.

KAEWNOPPARAT, S., SANSERNLUK, K. and FAROONGSARNG, D., 2008. Behavior of Freezable Bound Water in the Bacterial Cellulose Produced by Acetobacter xylinum: An Approach Using Thermoporosimetry. *AAPS PharmSciTech,* **9**(2), pp. 701-707.

KAY, W.B., 1968. Critical locus curve and the phase behavior of mixtures. *Accounts of Chemical Research,* **1**(11), pp. 344-351.

KHALIL, H.A., DAVOUDPOUR, Y., SAURABH, C.K., HOSSAIN, M.S., ADNAN, A., DUNGANI, R., PARIDAH, M., SARKER, M.Z.I., FAZITA, M.N. and SYAKIR, M., 2016. A review on nanocellulosic fibres as new material for sustainable packaging: Process and applications. *Renewable and Sustainable Energy Reviews,* **64**, pp. 823-836.

KIANI, H. and SUN, D., 2011. *Water crystallization and its importance to freezing of foods: A review.*

KIMURA, M., QI, Z.-. and ISOGAI, A., 2016. Analysis of mesopore structures in wood cell walls and pulp fibers by nitrogen adsorption method. *Nordic Pulp and Paper Research Journal,* **31**(2), pp. 198-204.

KIMURA, M., QI, Z., FUKUZUMI, H., KUGA, S. and ISOGAI, A., 2014. Mesoporous structures in never-dried softwood cellulose fibers investigated by nitrogen adsorption. *Cellulose,* **21**(5), pp. 3193-3201.

KLEMM, D., HEUBLEIN, B., FINK, H. and BOHN, A., 2005. Cellulose: Fascinating Biopolymer and Sustainable Raw Material. *Angewandte Chemie International Edition,* **44**(22), pp. 3358-3393.

KOCH, G., 2008. Raw Material for Pulp. *Handbook of Pulp.* Wiley-VCH Verlag GmbH, pp. 21-68.

KSIĄŻCZAK, A., RADOMSKI, A. and ZIELENKIEWICZ, T., 2003a. Nitrocellulose porosity - thermoporometry. *Journal of Thermal Analysis and Calorimetry,* **74**(2), pp. 559-568.

KSIĄŻCZAK, A., RADOMSKI, A. and ZIELENKIEWICZ, T., 2003b. Nitrocellulose porosity - thermoporometry. *Journal of Thermal Analysis and Calorimetry,* **74**(2), pp. 559-568.

LADAVOS, A.K., KATSOULIDIS, A.P., IOSIFIDIS, A., TRIANTAFYLLIDIS, K.S., PINNAVAIA, T.J. and POMONIS, P.J., 2012. *The BET equation, the inflection points of N2 adsorption isotherms and the estimation of specific surface area of porous solids.*

LANDERS, J., GOR, G.Y. and NEIMARK, A.V., 2013. Density functional theory methods for characterization of porous materials. *Colloids and Surfaces A: Physicochemical and Engineering Aspects,* **437**, pp. 3-32.

LANDRY, M.R., 2005. Thermoporometry by differential scanning calorimetry: experimental considerations and applications. *Thermochimica Acta,* **433**(1–2), pp. 27-50.

LINDSTROM, T., 1982. The effect of carboxyl groups and their ionic form during drying on the hornification of cellulose fibers. *Svensk Paperstidning,* **85**, pp. R146-R151.

LINDSTRÖM, T., 1986. The concept and measurement of fiber swelling. *Paper.Structure and Properties, Marcel Dekker, New York,* , pp. 75-97.

LOVIKKA, V.A., KHANJANI, P., VÄISÄNEN, S., VUORINEN, T. and MALONEY, T.C., 2016. Porosity of wood pulp fibers in the wet and highly open dry state. *Microporous and Mesoporous Materials,* **234**, pp. 326-335.

MAJDA, D., MAKOWSKI, W., MAŃKO, M., MLEKODAJ, K., MICHALIK-ZYM, A., NAPRUSZEWSKA, B.D., ZIMOWSKA, M. and SERWICKA, E.M., 2015. Porosity characterization of SBA-15 silicas with thermoporosimetry of water and n-alkanes – The effect of the probe liquid nature. *Microporous and Mesoporous Materials,* **201**, pp. 141-150.

MALCOLM JR, R. and SAXENA, I.M., 2007. Cellulose Shapes. *Cellulose: Molecular and Structural Biology: Selected Articles on the Synthesis, Structure, and Applications of Cellulose.* Springer Science & Business Media, pp. 259.

MALONEY, T. and PAULAPURO, H., 2001. Thermoporosimetry of pulp fibers, *The Science of Papermaking: Transactions of the 12th Fundamental Research Symposium in Held at Oxford* 2001, pp. 897-926.

MALONEY, T. and PAULAPURO, H., 1999. The formation of pores in the cell wall. *Journal of Pulp and Paper Science,* **25**(12), pp. 430-436.

MALONEY, T., 1999. Thermoporosimetry by isothermal step melting. *ISWPC Pre-symposium, Seoul, 1999.* Korea Tappi, pp. 245.

MALONEY, T., LAINE, J.E. and PAULAPURO, H., 1999. Comments on the measurement of cell wall water. *Tappi Journal,* **82**(9), pp. 125.

MALONEY, T.C., 2015. Thermoporosimetry of hard (silica) and soft (cellulosic) materials by isothermal step melting. *Journal of Thermal Analysis and Calorimetry,* **121**(1), pp. 7-17.

MALONEY, T.C., PAULAPURO, H. and STENIUS, P., 1998. Hydration and swelling of pulp fibers measured with differential scanning calorimetry. *Nordic Pulp & Paper Research Journal,* **13**(1), pp. 031-036.

MATTHIAS, T., KATSUMI, K., NEIMARK, A.V., OLIVIER, J.P., RODRIGUEZ-REINOSO FRANCISCO, JEAN, R. and SING, K.S., 2015. *Physisorption of gases, with special reference to the evaluation of surface area and pore size distribution (IUPAC Technical Report).*

MEYERS, J. and NANKO, H., 2005. Effects of fines on the fiber length and coarseness values measured by the fiber quality analyzer (FQA), *TAPPI Practical Papermaking Conference, Milwaukee, WI, USA* 2005.

MIAO, Q., CHEN, L., HUANG, L., TIAN, C., ZHENG, L. and NI, Y., 2014. *A process for enhancing the accessibility and reactivity of hardwood kraft-based dissolving pulp for viscose rayon production by cellulase treatment.*

MILANOVIC, J., KOSTIC, M., MILANOVIC, P. and SKUNDRIC, P., 2012. Influence of TEMPO-Mediated Oxidation on Properties of Hemp Fibers. *Industrial & Engineering Chemistry Research,* **51**(29), pp. 9750-9759.

MISTURA, G., POZZATO, A., GRENCI, G., BRUSCHI, L. and TORMEN, M., 2013. Continuous adsorption in highly ordered porous matrices made by nanolithography. **4**, pp. 2966.

MITCHELL, J., WEBBER, J.B.W. and STRANGE, J.H., 2008a. Nuclear magnetic resonance cryoporometry. *Physics Reports,* **461**(1), pp. 1-36.

MITCHELL, J., WEBBER, J.B.W. and STRANGE, J.H., 2008b. Nuclear magnetic resonance cryoporometry. *Physics Reports,* **461**(1), pp. 1-36.

NAKAMURA, K., HATAKEYAMA, T. and HATAKEYAMA, H., 1981a. Studies on bound water of cellulose by differential scanning calorimetry. *Textile Research Journal,* **51**(9), pp. 607-613.

NAKAMURA, K., HATAKEYAMA, T. and HATAKEYAMA, H., 1981b. Studies on Bound Water of Cellulose by Differential Scanning Calorimetry. *Textile Research Journal,* **51**(9), pp. 607-613.

NEVELL, T.P. and ZERONIAN, S.H., 1985. Cellulose chemistry and its applications.

PANDITHAGE, R., 2012. Brief Introduction to Critical Point Drying.

PARK, S., VENDITTI, R.A., JAMEEL, H. and PAWLAK, J.J., 2006. Changes in pore size distribution during the drying of cellulose fibers as measured by differential scanning calorimetry. *Carbohydrate Polymers,* **66**(1), pp. 97-103.

PASTORINO, D., CANAL, C. and GINEBRA, M., 2015. Multiple characterization study on porosity and pore structure of calcium phosphate cements. *Acta Biomaterialia,* **28**, pp. 205-214.

PENG, Y., GARDNER, D.J. and HAN, Y., 2012. Drying cellulose nanofibrils: in search of a suitable method. *Cellulose,* **19**(1), pp. 91-102.

PIERRE, A.C. and PAJONK, G.M., 2002. Chemistry of aerogels and their applications. *Chemical reviews,* **102**(11), pp. 4243-4265.

PLOMION, C., LEPROVOST, G. and STOKES, A., 2001. Wood Formation in Trees. *Plant Physiology,* **127**(4), pp. 1513-1523.

PÖNNI, R., VUORINEN, T. and KONTTURI, E., 2012a. Proposed nano-scale coalescence of cellulose in chemical pulp fibers during technical treatments. *BioResources,* **7**(4), pp. 6077-6108.

PÖNNI, R., VUORINEN, T. and KONTTURI, E., 2012b. Proposed nano-scale coalescence of cellulose in chemical pulp fibers during technical treatments. *BioResources,* **7**(4), pp. 6077-6108.

QUIRK, J., 1955. SIGNIFICANCE OF SURFACE AREAS CALCULATED FROM WATER VAPOR SORPTION ISOTHERMS BY USE OF THE BET EQUATION. *Soil Science,* **80**(6), pp. 423-430.

RIIKONEN, J., SALONEN, J. and LEHTO, V., 2011a. Utilising thermoporometry to obtain new insights into nanostructured materials. *Journal of Thermal Analysis and Calorimetry,* **105**(3), pp. 823-830.

RIIKONEN, J., SALONEN, J. and LEHTO, V., 2011b. Utilising thermoporometry to obtain new insights into nanostructured materials. *Journal of Thermal Analysis and Calorimetry,* **105**(3), pp. 811-821.

ROWELL, R.M., PETTERSEN, R., HAN, J.S., ROWELL, J.S. and TSHABALALA, M.A., 2005. Cell wall chemistry. *Handbook of wood chemistry and wood composites,* , pp. 35-74.

SCALLAN, A. and GRIGNON, J., 1979. The effect of cations on pulp and paper properties. *Svensk Papperstidning,* **2**, pp. 40-47.

SING, K.S.W., 2009. *Reporting physisorption data for gas/solid systems with special reference to the determination of surface area and porosity (Recommendations 1984).*

SJÖSTRÖM, E., 1993. The structure of wood. *Wood Chemistry-Fundamentals and Applications,* , pp. 5-16.

SJOSTROM, E., 2013. *Wood chemistry: fundamentals and applications.* Elsevier.

SLUITER, A., HAMES, B., RUIZ, R., SCARLATA, C., SLUITER, J., TEMPLETON, D. and CROCKER, D., 2008. Determination of Structural Carbohydrates and Lignin in Biomass. *NREL Technical Report, .*

STAPF, S., KIMMICH, R., SEITTER, R.-., MAKLAKOV, A.I. and SKIRDA, V.D., 1996. *Proton and deuteron field-cycling NMR relaxometry of liquids confined in porous glasses.*

STONE, J. and SCALLAN, A., 1968. A structural model for the cell wall of water-swollen wood pulp fibres based on their accessibility to macromolecules. *Cellulose Chemistry and Technology,* **2**, pp. 343-358.

STONE, J.E. and SCALLAN, A.M., 1965. Effect of component removal upon the porous structure of the cell wall of wood. *Journal of Polymer Science Part C: Polymer Symposia,* **11**(1), pp. 13-25.

SWEET, M.S. and WINANDY, J.E., 1999. Influence of degree of polymerization of cellulose and hemicellulose on strength loss in fire-retardant-treated southern pine. *Holzforschung,* **53**(3), pp. 311-317.

THOMMES, M. and CYCHOSZ, K.A., 2014. Physical adsorption characterization of nanoporous materials: progress and challenges. *Adsorption,* **20**(2), pp. 233-250.

VALIULLIN, R., 2014. NMR Cryoporometry and Estimation of Pore Sizes in Mesoporous Silicon. In: L. CANHAM, ed, *Handbook of Porous Silicon.* Cham: Springer International Publishing, pp. 439-447.

VARSHNEY, V. and NAITHANI, S., 2011. Chemical functionalization of cellulose derived from nonconventional sources. *Cellulose Fibers: Bio-and Nano-Polymer Composites.* Springer, pp. 43-60.

VIEL, S., CAPITANI, D., PROIETTI, N., ZIARELLI, F. and SEGRE, A.L., 2004. NMR spectroscopy applied to the Cultural Heritage: A preliminary study on ancient wood characterisation. *Applied Physics A: Materials Science and Processing,* **79**(2), pp. 357-361.

WANG, X., 2006. *Improving the papermaking properties of kraft pulp by controlling hornification and internal fibrillation*, Helsinki University of Technology; Teknillinen korkeakoulu.

WEBBER, J.B.W., STRANGE, J.H. and DORE, J.C., 2001. An evaluation of NMR cryoporometry, density measurement and neutron scattering methods of pore characterisation. *Magnetic resonance imaging,* **19**(3-4), pp. 395-399.

WEITKAMP, J., SING, K.S.W. and SCHÜTH, F., 2002. *Handbook of porous solids.* Wiley-Vch Weinheim.

WU, J., ZHENG, H., CHENG, H., ZHOU, L., LEONG, K.C., RAJAGOPALAN, R., TOO, H.P. and CHOI, W.K., 2014. Thermoporometry Characterization of Silica Microparticles and Nanowires. *Langmuir,* **30**(8), pp. 2206-2215.

WULFF, M., 2004a. Pore size determination by thermoporometry using acetonitrile. *Thermochimica Acta,* **419**(1–2), pp. 291-294.

WULFF, M., 2004b. Pore size determination by thermoporometry using acetonitrile. *Thermochimica Acta,* **419**(1–2), pp. 291-294.

YAMAMOTO, T., ENDO, A., INAGI, Y., OHMORI, T. and NAKAIWA, M., 2005. Evaluation of thermoporometry for characterization of mesoporous materials. *Journal of colloid and interface science,* **284**(2), pp. 614-620.

APPENDIX 1: Determination of corrected Gibbs-Thomson coefficient

Corrected Gibbs-Thomson coefficient was calculated from thermoporosimetry and Hg-porosimetry. See Table 8 and section 5.8

		USW-K-ND			
1/ΔT	**ΔT (°C)**	**Cumulative volume from Thermoporosimetry (mL/g)**	**Diameter from Thermoporosimetry (nm)**	**Diameter from Hg-porosimetry (nm)**	**Cumulative Volume (mL/g)**
0,08	12,50	0,00	77,00	77,00	0,00
0,10	10,50	0,01	81,17	85,70	0,02
0,12	8,50	0,03	90,25	95,30	0,04
0,13	7,50	0,04	95,02	106,00	0,06
0,15	6,50	0,05	100,79	117,90	0,08
0,18	5,50	0,06	108,61	131,10	0,09
0,22	4,50	0,07	119,08	145,90	0,11
0,29	3,50	0,09	132,14	162,20	0,12
0,40	2,50	0,11	153,45	180,40	0,13
0,67	1,50	0,13	192,07	200,70	0,14
1,00	1,00	0,15	227,68	223,20	0,15
1,43	0,70	0,16	265,67	276,20	0,17
2,00	0,50	0,18	317,09	248,30	0,17
3,33	0,30	0,21	474,57	307,10	0,18
5,00	0,20	0,25	773,75	380,00	0,19
				341,60	0,19
				422,60	0,20
				470,00	0,21
				522,80	0,22
				581,50	0,22
				646,70	0,23
				719,30	0,24
				800,10	0,25
				889,90	0,27
				989,70	0,28
				1100,80	0,30
				1224,40	0,32
				1361,80	0,33
				1514,60	0,35
				1684,60	0,39

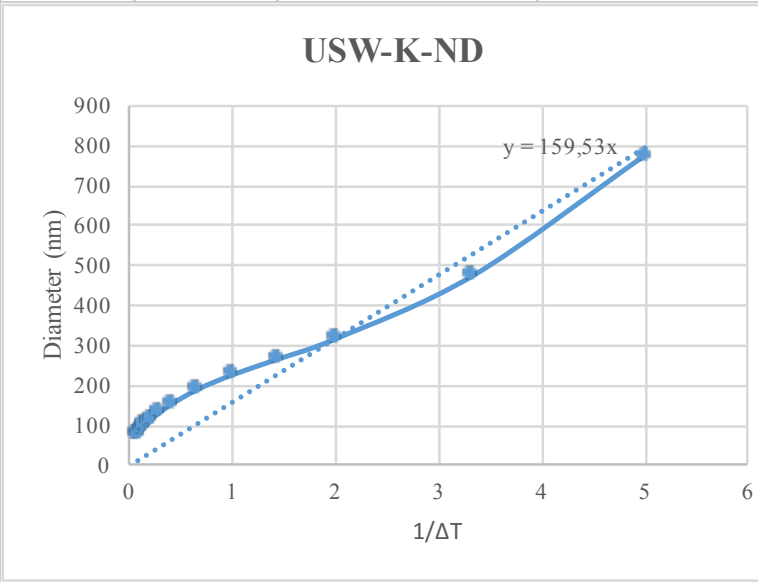

USW-K-D

1/ΔT	ΔT (°C)	Cumulative volume from Thermoporosimetry (mL/g)	Diameter from Thermoporosimetry (nm)	Diameter from Hg-porosimetry (nm)	Cumulative Volume (mL/g)
0,08	12,50	0,00	29,60	29,60	0,00
0,10	10,50	0,01	30,62	32,90	0,03
0,12	8,50	0,02	32,40	36,60	0,06
0,13	7,50	0,03	33,51	40,70	0,09
0,15	6,50	0,04	34,78	45,30	0,13
0,18	5,50	0,05	36,19	50,30	0,15
0,22	4,50	0,07	37,91	56,00	0,17
0,29	3,50	0,08	39,89	62,30	0,19
0,40	2,50	0,10	42,65	69,30	0,21
0,67	1,50	0,12	47,10	77,00	0,22
1,00	1,00	0,14	50,46	85,70	0,23
1,43	0,70	0,16	54,31	95,30	0,23
2,00	0,50	0,17	59,24	117,90	0,24
3,33	0,30	0,20	74,84	106,00	0,24
5,00	0,20	0,25	134,25	131,10	0,25
				145,90	0,26
				162,20	0,26
				180,40	0,27
				200,70	0,27
				223,20	0,28
				276,20	0,29
				248,30	0,29
				307,10	0,29
				341,60	0,30
				380,00	0,30
				422,60	0,31
				522,80	0,32
				470,00	0,32
				581,50	0,32
				646,70	0,33
				719,30	0,34
				800,10	0,34
				989,70	0,35
				889,90	0,35
				1100,80	0,35
				1224,40	0,36

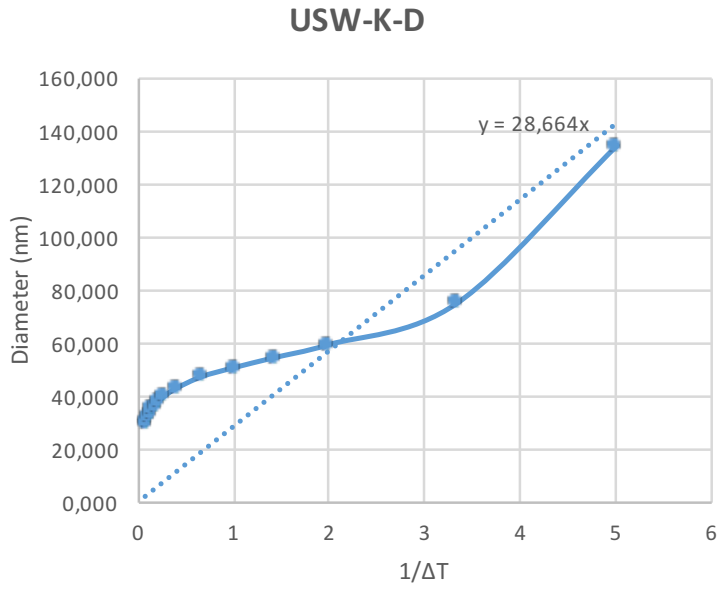

BHW-K-ND

1/ΔT	ΔT (°C)	Cumulative volume from Thermoporosimetry (mL/g)	Diameter from Thermoporosimetry (nm)	Diameter from Hg-porosimetry (nm)	Cumulative Volume (mL/g)
0,08	12,50	0,00	45,30	45,30	0,00
0,10	10,50	0,01	47,92	50,30	0,02
0,12	8,50	0,03	53,55	56,00	0,05
0,13	7,50	0,05	57,20	62,30	0,06
0,15	6,50	0,06	62,62	69,30	0,09
0,18	5,50	0,08	70,28	77,00	0,10
0,22	4,50	0,11	80,74	85,70	0,12
0,29	3,50	0,13	95,64	95,30	0,14
0,40	2,50	0,17	121,79	106,00	0,16
0,67	1,50	0,22	178,76	117,90	0,17
1,00	1,00	0,25	233,50	131,10	0,18
1,43	0,70	0,28	294,68	145,90	0,20
2,00	0,50	0,31	369,67	162,20	0,21
3,33	0,30	0,35	512,24	180,40	0,23
5,00	0,20	0,40	656,35	200,70	0,24
				223,20	0,26
				248,30	0,26
				276,20	0,28
				307,10	0,29
				341,60	0,30
				380,00	0,32
				422,60	0,33
				470,00	0,35
				522,80	0,36
				581,50	0,38
				646,70	0,39
				719,30	0,41
				800,10	0,44
				889,90	0,48
				989,70	0,51

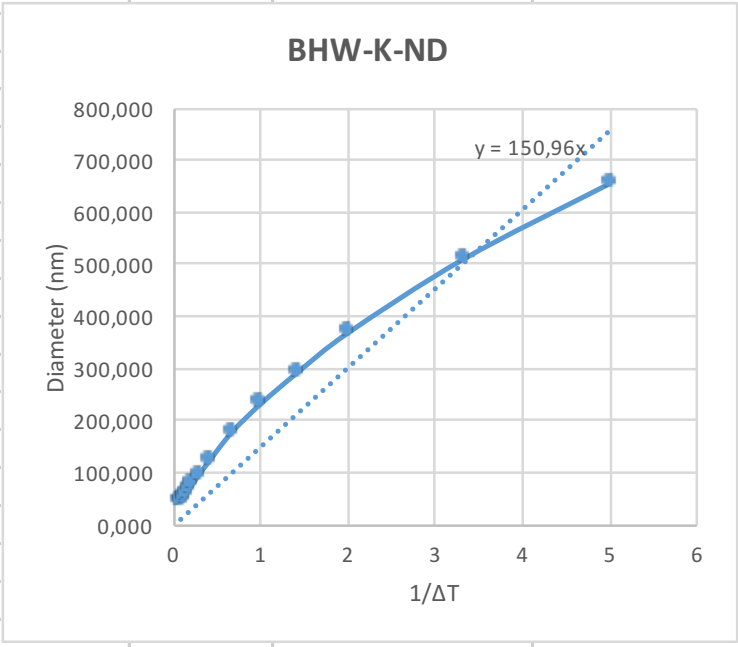

BHW-dD

1/ΔT	ΔT (°C)	Cumulative volume from Thermoporosimetry (mL/g)	Diameter from Thermoporosimetry (nm)	Diameter from Hg-porosimetry (nm)	Cumulative Volume (mL/g)
0,08	12,50	0,00	10,20	10,20	0,00
0,10	10,50	0,01	10,41	11,40	0,03
0,12	8,50	0,02	10,84	12,60	0,07
0,13	7,50	0,03	11,10	14,00	0,10
0,15	6,50	0,03	11,38	15,60	0,13
0,18	5,50	0,04	11,75	17,40	0,15
0,22	4,50	0,05	12,19	19,30	0,18
0,29	3,50	0,07	12,78	21,50	0,20
0,40	2,50	0,08	13,57	23,90	0,21
0,67	1,50	0,11	15,03	26,60	0,23
1,00	1,00	0,13	16,39	29,60	0,24
1,43	0,70	0,15	18,09	32,90	0,25
2,00	0,50	0,18	20,74	36,60	0,27
3,33	0,30	0,24	30,45	40,70	0,28
5,00	0,20	0,31	55,41	45,30	0,29
				50,30	0,30
				56,00	0,31
				62,30	0,32
				77,00	0,34
				69,30	0,34
				85,70	0,36
				95,30	0,36
				106,00	0,38
				117,90	0,40
				131,10	0,41
				145,90	0,42
				162,20	0,44
				180,40	0,45
				200,70	0,46

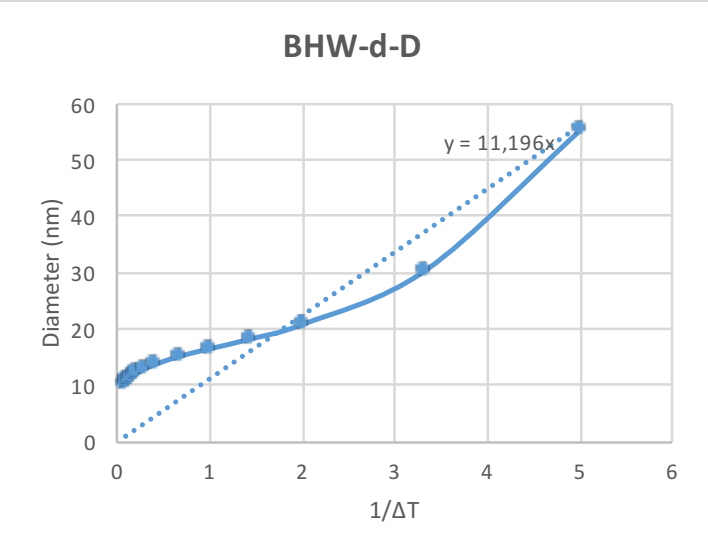

		TEMPO			
1/ΔT	ΔT (°C)	**Cumulative volume from Thermoporosimetry (mL/g)**	**Diameter from Thermoporosimetry (nm)**	**Diameter from Hg-porosimetry (nm)**	**Cumulative Volume (mL/g)**
0,08	12,50	0,00	40,70	40,70	0,00
0,10	10,50	0,01	44,08	45,30	0,02
0,12	8,50	0,04	51,14	50,30	0,04
0,13	7,50	0,05	56,21	56,00	0,06
0,15	6,50	0,08	63,66	62,30	0,08
0,18	5,50	0,11	76,53	69,30	0,09
0,22	4,50	0,14	97,84	77,00	0,12
0,29	3,50	0,20	139,95	85,70	0,13
0,40	2,50	0,28	229,07	95,30	0,15
0,67	1,50	0,41	426,29	106,00	0,16
1,00	1,00	0,49	599,47	117,90	0,17
1,43	0,70	0,55	759,27	131,10	0,20
2,00	0,50	0,61	930,52	145,90	0,21
3,33	0,30	0,72	1284,96	162,20	0,23
5,00	0,20	0,83	1714,10	180,40	0,25
				200,70	0,26
				223,20	0,28
				248,30	0,30
				276,20	0,32
				307,10	0,35
				341,60	0,37
				380,00	0,39
				422,60	0,42
				470,00	0,44
				522,80	0,46
				581,50	0,49
				646,70	0,52
				719,30	0,54
				800,10	0,56
				889,90	0,60
				989,70	0,63
				1100,80	0,65
				1224,40	0,73
				1361,80	0,75
				1514,60	0,81
				1684,60	0,86
				1873,70	0,91

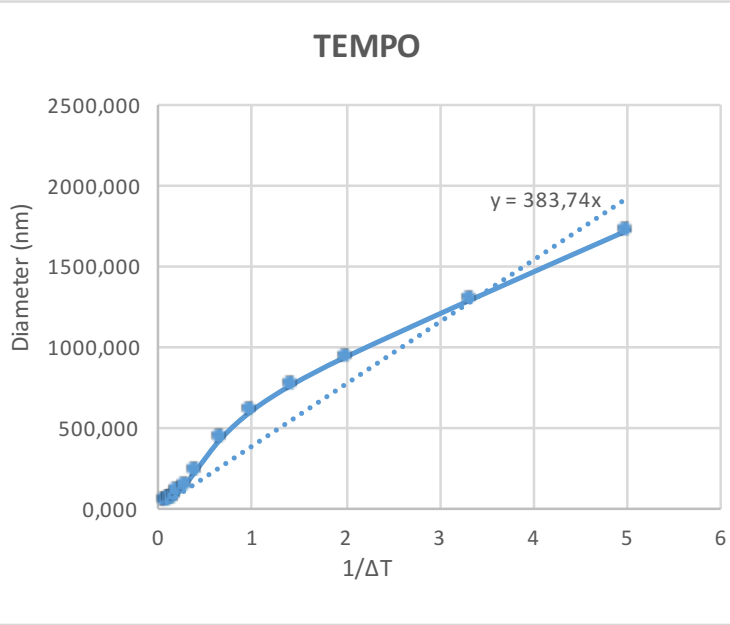

				APPENDIX I (6/6)	
TEMPO					
				Diameter from Hg-porosimetry (nm)	**Cumulative Volume (mL/g)**
				2084,00	0,92
				2317,90	0,95
				2578,10	0,97
				2867,50	0,98
				3189,30	0,99
				3547,30	1,00
				3945,40	1,04
				4388,20	1,08
				4880,80	1,13

APPENDIX II: Pore size distribution from N2 sorption

See section 5.5

USW-K-ND		USW-K-D	
Pore width (nm)	Pore volume (mL/g)	Pore width (nm)	Pore volume (mL/g)
83,47	0,63	86,84	0,48
68,10	0,62	68,87	0,48
53,86	0,62	53,85	0,47
41,49	0,61	41,79	0,47
36,33	0,60	36,45	0,46
29,36	0,59	29,62	0,46
25,99	0,57	25,78	0,45
21,41	0,56	21,56	0,44
18,55	0,54	18,58	0,43
15,92	0,51	15,86	0,42
13,67	0,49	13,66	0,41
12,26	0,45	12,36	0,39
10,59	0,42	10,61	0,37
9,37	0,37	9,36	0,34
8,69	0,33	8,69	0,32
7,64	0,31	7,64	0,30
6,75	0,26	6,74	0,26
6,22	0,22	6,22	0,23
5,67	0,19	5,68	0,21
5,30	0,17	5,30	0,18
4,81	0,15	4,81	0,16
4,44	0,12	4,44	0,14
4,26	0,10	4,25	0,12
4,08	0,09	4,08	0,11
3,88	0,08	3,88	0,10
3,76	0,07	3,77	0,09
3,57	0,06	3,57	0,08
3,39	0,05	3,39	0,07
3,16	0,05	3,16	0,06
2,86	0,03	2,86	0,05
2,65	0,02	2,65	0,03
2,48	0,01	2,48	0,02
2,35	0,01	2,35	0,01
2,22	0,01	2,22	0,01
2,11	0,00	2,11	0,01
2,01	0,00	2,01	0,00
		1,90	0,00
		1,78	0,00

			APPENDIX II (2/3)
	BHW-K-ND		**BHW-dD**
Pore width (nm)	Pore volume (mL/g)	Pore width (nm)	Pore volume (mL/g)
81,73	0,49	83,72	0,16
64,66	0,48	67,51	0,16
52,44	0,47	53,87	0,15
40,74	0,46	42,00	0,15
35,69	0,44	36,69	0,14
29,12	0,43	29,75	0,14
25,49	0,41	26,02	0,14
21,14	0,40	21,52	0,13
18,39	0,37	18,78	0,13
15,78	0,36	16,02	0,12
13,59	0,33	13,74	0,12
12,24	0,31	12,45	0,11
10,56	0,29	10,70	0,11
9,36	0,26	9,40	0,10
8,66	0,23	8,77	0,10
7,62	0,21	7,71	0,09
6,74	0,18	6,77	0,09
6,22	0,16	6,25	0,08
5,67	0,14	5,69	0,08
5,30	0,12	5,32	0,07
4,81	0,11	4,83	0,06
4,44	0,09	4,45	0,06
4,26	0,07	4,26	0,05
4,09	0,07	4,09	0,05
3,88	0,06	3,88	0,04
3,77	0,05	3,77	0,04
3,57	0,05	3,57	0,04
3,39	0,04	3,39	0,03
3,16	0,03	3,16	0,03
2,86	0,02	2,86	0,02
2,65	0,01	2,65	0,02
2,48	0,01	2,48	0,01
2,35	0,00	2,35	0,01
2,22	0,00	2,22	0,01
2,12	0,00	2,12	0,00
2,01	0,00	2,01	0,00
		1,90	0,00
		1,78	0,00
		1,64	0,00

			APPENDIX II (3/3)
TEMPO			
Pore width (nm)	Pore volume (mL/g)		
83,92	0,45		
66,54	0,44		
53,85	0,42		
41,66	0,39		
36,75	0,37		
29,92	0,36		
25,98	0,34		
21,44	0,32		
18,75	0,30		
15,98	0,28		
13,74	0,26		
12,42	0,24		
10,70	0,23		
9,38	0,21		
8,75	0,19		
7,69	0,18		
6,78	0,16		
6,24	0,14		
5,70	0,12		
5,32	0,11		
4,83	0,10		
4,46	0,08		
4,27	0,07		
4,09	0,06		
3,89	0,06		
3,78	0,05		
3,58	0,05		
3,40	0,04		
3,16	0,03		
2,87	0,03		
2,65	0,02		
2,49	0,01		
2,35	0,01		
2,22	0,00		
2,12	0,00		
2,02	0,00		

APPENDIX III: Pore size distribtution from Hg-porosimetry									
See section 5.6								APPENDIX III (1/3)	
PW= Pore Width (nm)									
PV=Pore Volume (mL/g)									
USW-K-ND		USW-K-D		BHW-K-ND		BHW-d-D		TEMPO	
PW	PV	PW	PV	PW	PV	PW	PV	PW	PV
3,20	0,00	3,20	0,00	3,20	0,00	3,20	0,00	3,20	0,00
3,50	0,00	3,50	0,00	3,50	0,00	3,50	0,00	3,50	0,00
3,90	0,00	3,90	0,00	3,90	0,00	3,90	0,00	3,90	0,00
4,40	0,01	4,40	0,00	4,40	0,01	4,40	0,00	4,40	0,00
4,80	0,02	4,80	0,00	4,80	0,03	4,80	0,00	4,80	0,01
5,40	0,05	5,40	0,00	5,40	0,03	5,40	0,00	5,40	0,01
6,00	0,06	6,00	0,00	6,00	0,03	6,00	0,00	6,00	0,01
6,70	0,08	6,70	0,00	6,70	0,05	6,70	0,01	6,70	0,04
7,40	0,09	7,40	0,00	7,40	0,06	7,40	0,02	7,40	0,06
8,30	0,11	8,30	0,01	8,30	0,08	8,30	0,03	8,30	0,08
9,20	0,12	9,20	0,03	9,20	0,10	9,20	0,05	9,20	0,10
10,20	0,13	10,20	0,07	10,20	0,12	10,20	0,08	10,20	0,12
11,40	0,14	11,40	0,10	11,40	0,14	11,40	0,11	11,40	0,15
12,60	0,16	12,60	0,15	12,60	0,17	12,60	0,14	12,60	0,17
14,00	0,17	14,00	0,19	14,00	0,19	14,00	0,18	14,00	0,19
15,60	0,18	15,60	0,23	15,60	0,21	15,60	0,21	15,60	0,21
17,40	0,21	17,40	0,24	17,40	0,23	17,40	0,23	17,40	0,23
19,30	0,23	19,30	0,28	19,30	0,26	19,30	0,26	19,30	0,25
21,50	0,25	21,50	0,31	21,50	0,30	21,50	0,27	21,50	0,29
23,90	0,28	23,90	0,35	23,90	0,33	23,90	0,29	23,90	0,33
26,60	0,30	26,60	0,39	26,60	0,36	26,60	0,31	26,60	0,35
29,60	0,34	29,60	0,41	29,60	0,39	29,60	0,32	29,60	0,38
32,90	0,37	32,90	0,44	32,90	0,41	32,90	0,33	32,90	0,40
36,60	0,40	36,60	0,47	36,60	0,43	36,60	0,35	36,60	0,43
40,70	0,43	40,70	0,50	40,70	0,46	40,70	0,36	40,70	0,45
45,30	0,46	45,30	0,54	45,30	0,49	45,30	0,37	45,30	0,47
50,30	0,49	50,30	0,56	50,30	0,51	50,30	0,37	50,30	0,48
56,00	0,53	56,00	0,58	56,00	0,53	56,00	0,39	56,00	0,51
62,30	0,56	62,30	0,60	62,30	0,55	62,30	0,40	62,30	0,52
69,30	0,58	69,30	0,62	69,30	0,57	69,30	0,42	69,30	0,54
77,00	0,61	77,00	0,63	77,00	0,59	77,00	0,42	77,00	0,57
85,70	0,63	85,70	0,64	85,70	0,61	85,70	0,43	85,70	0,58
95,30	0,65	95,30	0,64	95,30	0,62	95,30	0,44	95,30	0,59
106,00	0,67	106,00	0,65	106,00	0,64	106,00	0,46	106,00	0,61
117,90	0,69	117,90	0,65	117,90	0,66	117,90	0,47	117,90	0,62
131,10	0,70	131,10	0,66	131,10	0,67	131,10	0,48	131,10	0,65
145,90	0,72	145,90	0,67	145,90	0,69	145,90	0,50	145,90	0,66
162,20	0,73	162,20	0,67	162,20	0,70	162,20	0,52	162,20	0,68
180,40	0,74	180,40	0,68	180,40	0,71	180,40	0,53	180,40	0,70

APPENDIX III (2/3)

USW-K-ND		USW-K-D		BHW-K-ND		BHW-d-D		TEMPO	
PW	PV	PW	PV	PW	PV	PW	PV	PW	PV
200,70	0,75	200,70	0,68	200,70	0,72	200,70	0,53	200,70	0,71
223,20	0,76	223,20	0,69	223,20	0,74	223,20	0,55	223,20	0,73
248,30	0,78	248,30	0,70	248,30	0,75	248,30	0,56	248,30	0,75
276,20	0,78	276,20	0,70	276,20	0,77	276,20	0,57	276,20	0,77
307,10	0,79	307,10	0,70	307,10	0,78	307,10	0,57	307,10	0,80
341,60	0,80	341,60	0,71	341,60	0,79	341,60	0,58	341,60	0,81
380,00	0,80	380,00	0,71	380,00	0,80	380,00	0,60	380,00	0,84
422,60	0,81	422,60	0,72	422,60	0,81	422,60	0,60	422,60	0,86
470,00	0,82	470,00	0,73	470,00	0,83	470,00	0,61	470,00	0,89
522,80	0,83	522,80	0,73	522,80	0,84	522,80	0,61	522,80	0,91
581,50	0,83	581,50	0,73	581,50	0,86	581,50	0,61	581,50	0,94
646,70	0,84	646,70	0,74	646,70	0,87	646,70	0,62	646,70	0,97
719,30	0,85	719,30	0,74	719,30	0,89	719,30	0,63	719,30	0,99
800,10	0,87	800,10	0,75	800,10	0,93	800,10	0,64	800,10	1,01
889,90	0,88	889,90	0,76	889,90	0,96	889,90	0,65	889,90	1,05
989,70	0,89	989,70	0,76	989,70	0,99	989,70	0,66	989,70	1,07
1100,80	0,91	1100,80	0,76	1100,80	1,03	1100,80	0,66	1100,80	1,10
1224,40	0,93	1224,40	0,77	1224,40	1,08	1224,40	0,67	1224,40	1,18
1361,80	0,94	1361,80	0,78	1361,80	1,12	1361,80	0,68	1361,80	1,20
1514,60	0,96	1514,60	0,79	1514,60	1,17	1514,60	0,68	1514,60	1,26
1684,60	1,00	1684,60	0,80	1684,60	1,22	1684,60	0,69	1684,60	1,31
1873,70	1,01	1873,70	0,83	1873,70	1,24	1873,70	0,69	1873,70	1,35
2084,00	1,04	2084,00	0,85	2084,00	1,25	2084,00	0,70	2084,00	1,37
2317,90	1,06	2317,90	0,86	2317,90	1,27	2317,90	0,70	2317,90	1,40
2578,10	1,08	2578,10	0,88	2578,10	1,27	2578,10	0,70	2578,10	1,42
2867,50	1,09	2867,50	0,89	2867,50	1,28	2867,50	0,70	2867,50	1,42
3189,30	1,10	3189,30	0,90	3189,30	1,28	3189,30	0,71	3189,30	1,44
3547,30	1,12	3547,30	0,91	3547,30	1,28	3547,30	0,71	3547,30	1,45
3945,40	1,15	3945,40	0,93	3945,40	1,29	3945,40	0,73	3945,40	1,49
4388,20	1,19	4388,20	0,96	4388,20	1,31	4388,20	0,74	4388,20	1,53
4880,80	1,23	4880,80	0,98	4880,80	1,32	4880,80	0,76	4880,80	1,58
5428,60	1,25	5428,60	1,01	5428,60	1,34	5428,60	0,78	5428,60	1,63
6037,90	1,28	6037,90	1,03	6037,90	1,36	6037,90	0,79	6037,90	1,70
6715,60	1,31	6715,60	1,05	6715,60	1,38	6715,60	0,81	6715,60	1,76
7469,30	1,33	7469,30	1,06	7469,30	1,41	7469,30	0,85	7469,30	1,83
8307,60	1,36	8307,60	1,08	8307,60	1,43	8307,60	0,88	8307,60	1,91
9240,10	1,38	9240,10	1,11	9240,10	1,47	9240,10	0,93	9240,10	1,99
10277,20	1,41	10277,20	1,13	10277,20	1,50	10277,20	0,97	10277,20	2,10
11430,70	1,44	11430,70	1,16	11430,70	1,54	11430,70	1,03	11430,70	2,20

APPENDIX III (3/3)

USW-K-ND		USW-K-D		BHW-K-ND		BHW-d-D		TEMPO	
PW	PV	PW	PV	PW	PV	PW	PV	PW	PV
12713,60	1,47	12713,60	1,19	12713,60	1,59	12713,60	1,11	12713,60	2,32
14140,60	1,51	14140,60	1,23	14140,60	1,64	14140,60	1,21	14140,60	2,44
15727,70	1,56	15727,70	1,27	15727,70	1,71	15727,70	1,32	15727,70	2,57
17493,00	1,61	17493,00	1,31	17493,00	1,79	17493,00	1,48	17493,00	2,71
19456,30	1,66	19456,30	1,36	19456,30	1,88	19456,30	1,66	19456,30	2,85
21640,10	1,74	21640,10	1,42	21640,10	2,01	21640,10	1,87	21640,10	3,00
24068,90	1,82	24068,90	1,49	24068,90	2,17	24068,90	2,13		
26770,40	1,91	26770,40	1,58	26770,40	2,36	26770,40	2,46		
29775,10	2,03	29775,10	1,70	29775,10	2,63	29775,10	2,79		
33117,00	2,17	33117,00	1,83	33117,00	2,93	33117,00	3,19		
36834,00	2,34	36834,00	2,00						
40968,10	2,58	40968,10	2,21						
45566,30	2,87	45566,30	2,51						
50680,60	3,26	50680,60	2,88						

APPENDIX IV: Data from thermoporosimetry

CPD dried				Without drying			
USW-k-ND							
Chex content	Cumulative pore volume (mL/g)	NFC(mL/g)	Total pore volume (mL/g)	Chex content	Cumulative pore volume (mL/g)	NFC(mL/g)	Total pore volume (mL/g)
3,26	0,40	0,85	1,25	2,33	0,45	0,70	1,15
1,80	0,30	0,66	0,96	1,88	0,25	0,70	0,95
2,99	0,34	0,51	0,85	2,09	0,13	0,68	0,81
1,43	0,40	0,63	1,03	1,87	0,17	0,57	0,74
Average	0,36	0,66	1,02	2,31	0,20	0,37	0,57
SD (±)	0,05	0,14	0,17	2,71	0,55	0,75	1,30
				1,94	0,35	0,75	1,10
				Average	0,30	0,65	0,95
				SD (±)	0,16	0,14	0,26
USW-k-D							
1,14	0,28	0,53	0,81	1,94	0,13	0,27	0,40
1,58	0,50	0,29	0,79	1,29	0,26	0,51	0,77
1,66	0,36	0,43	0,79	1,79	0,28	0,51	0,79
2,50	0,31	0,07	0,38	1,92	0,18	0,32	0,50
2,09	0,40	0,51	0,91	1,88	0,25	0,27	0,52
1,91	0,30	0,44	0,74	1,49	0,35	0,47	0,82
Average	0,36	0,38	0,74	1,05	0,27	0,48	0,75
SD (±)	0,08	0,17	0,18	Average	0,25	0,40	0,65
				SD (±)	0,07	0,11	0,17
BHW-k-ND							
2,84	0,65	0,49	1,14	2,05	0,33	0,71	1,04
2,50	0,45	0,49	0,94	2,48	0,27	0,56	0,83
2,65	0,50	0,18	0,68	1,71	0,30	0,45	0,75
1,46	0,45	0,46	0,91	1,90	0,23	0,59	0,82
2,14	0,45	0,37	0,82	1,90	0,25	0,58	0,83
2,33	0,46	0,44	0,90	1,62	0,44	0,55	0,99
2,16	0,40	0,45	0,85	1,89	0,32	0,57	0,89
2,78	0,52	0,38	0,90	1,55	0,38	0,56	0,94
Average	0,49	0,41	0,89	Average	0,32	0,57	0,89
SD (±)	0,08	0,10	0,13	SD (±)	0,07	0,07	0,10

APPENDIX IV (2/2)

CPD dried				Without drying			
BHW-d-D							
Chex content	Cumulative pore volume (mL/g)	NFC (mL/g)	Total pore volume (mL/g)	Chex content	Cumulative pore volume (mL/g)	NFC (mL/g)	Total pore volume (mL/g)
1,18	0,50	0,10	0,60	1,66	0,27	0,10	0,37
1,48	0,42	-0,06	0,36	1,85	0,50	-0,01	0,49
2,14	0,50	-0,09	0,41	1,25	0,40	0,14	0,54
1,58	0,45	0,18	0,63	1,18	0,38	0,16	0,54
1,56	0,42	0,14	0,56	1,93	0,38	0,15	0,53
1,61	0,43	0,09	0,52	Average	0,39	0,11	0,49
Average	0,45	0,06	0,51	SD (±)	0,08	0,07	0,07
SD (±)	0,04	0,11	0,11				
TEMPO							
1,63	1,10	0,32	1,42	1,91	0,50	0,23	0,73
1,49	1,30	0,29	1,59	2,05	0,45	0,30	0,75
1,83	1,28	0,04	1,32	1,64	0,50	0,28	0,78
2,26	1,20	1,08	2,28	1,18	0,50	0,48	0,98
1,06	0,95	0,46	1,41	1,32	0,48	0,31	0,79
Average	1,17	0,44	1,60	Average	0,49	0,32	0,81
SD (±)	0,14	0,39	0,39	SD (±)	0,02	0,09	0,10
SD = standard deviation							